8-2016

Development of a fluidic mixing nozzle for 3D bioprinting

Will Hoggatt
Purdue University

Graduate School Form
30 Updated 12/26/2015

PURDUE UNIVERSITY
GRADUATE SCHOOL
Thesis/Dissertation Acceptance

This is to certify that the thesis/dissertation prepared

By William Hoggatt

Entitled

DEVELOPMENT OF A FLUIDIC MIXING NOZZLE FOR 3D BIOPRINTING

For the degree of Master of Science in Biomedical Engineering

Is approved by the final examining committee:

Sherry L. Voytik-Harbin
Chair

Pavlos P. Vlachos

Jenna L. Rickus

Hyowon Lee

To the best of my knowledge and as understood by the student in the Thesis/Dissertation Agreement, Publication Delay, and Certification Disclaimer (Graduate School Form 32), this thesis/dissertation adheres to the provisions of Purdue University's "Policy of Integrity in Research" and the use of copyright material.

Approved by Major Professor(s): Sherry L. Voytik-Harbin

Approved by: George R. Wodicka 7/27/2016

Head of the Departmental Graduate Program Date

DEVELOPMENT OF A FLUIDIC MIXING NOZZLE FOR 3D BIOPRINTING

A Thesis

Submitted to the Faculty

of

Purdue University

by

Will Hoggatt

In Partial Fulfillment of the

Requirements for the Degree

of

Master of Science in Biomedical Engineering

August 2016

Purdue University

West Lafayette, Indiana

I would like to dedicate this work to my family, friends, and myself. Nice job, everyone.

ACKNOWLEDGMENTS

I would first like to thank my advisor, Professor Sherry L. Voytik-Harbin, for seeing in me what few others bothered to see. Also for putting up with my blatant disregard for authority, humility, and the scientific method. I will be forever grateful of this opportunity that she gave me.

I would also like to acknowledge the other members of the Harbin lab, whose constant support and comradery helped me through the most trying times of the last few years. This work and my constant, cheerful demeanor would not have been possible without Kevin Buno, TJ Puls, Nimisha Bajaj, Rucha Joshi, Sarah Brookes, Lauren Watkins, Clarissa Hernandez, Zach Nelson, and the constant support and advice of David McMillan.

“Success is walking from failure to failure with no loss of enthusiasm.”

-Winston Churchill

TABLE OF CONTENTS

LIST OF TABLES

Table Page

LIST OF FIGURES

Figure Page

Figure Page

ABSTRACT

Hoggatt, William F. M.S.B.M.E., Purdue University, August, 2016. Development of a Fluidic Mixing Nozzle for 3D Bioprinting. Major Professor: Sherry L. Voytik-Harbin.

3D bioprinting is a relatively new and very promising field that uses conventional 3D printing techniques and adapts them to print biological materials that are suited for use with cells. These bioprinters can be used to print cells encapsulated within biological "ink" (bio-ink) to create and customize complex three-dimensional tissues and organs. Our work has focused on developing a new bioprinter nozzle that addresses critical gaps with present-day bioprinters, namely, the lack of standardized, physiologically-relevant biomaterials, and their one nozzle per composition printing capacity. These shortcomings preclude printing a range of cellular and biomaterial compositions (including gradients of cells and matrix components) within a single tissue construct.

Type I collagen oligomers, a new soluble collagen subdomain that falls between molecular and fibrillar size scales, are ideally suited for tissue fabrication. This collagen formulation, which is produced according to an ASTM voluntary consensus standard, i) exhibits rapid suprafibrillar self-assembly yielding highly interconnected collagen-fibril matrices resembling those found in the body's tissues, ii) supports cell encapsulation, and iii) allows customized, multi-scale design across the broadest range of tissue architectures and physical properties. These properties, along with its superior physiologic relevance,

support the use of this biomaterial in the development of a bioprinting nozzle that is able to address the key gaps in the field of 3D bioprinting.

After researching microfluidic mixing devices and current bioprinters, early iterations of a 3D bioprinting nozzle were designed and machined to mix three fundamental reagents required to form a broad array of collagen-fibril matrix compositions, namely oligomeric type I collagen (oligomer), oligomer diluent (diluent), and self-assembly reagent (S.A.R). The nozzle was designed to mix specified proportions of these solutions using a combination of hydrodynamic focusing and twisted channel mixing mechanisms before depositing the self-assembling collagen. Three syringe pumps were used to continuously drive varying flow rates of the three reagents to the nozzle, which allowed for the creation of a broad array of cell and matrix compositions, including fibril-density gradients.

To validate nozzle performance, three experiments were conducted to define dispensing volume accuracy and precision, mixing quality, and functional performance of dispensed materials, including cells and matrix.

In summary, the integration of standardized self-assembling collagens with this innovative fluidic mixer effectively minimizes the number of printing reservoirs, employs a single dispensing nozzle, and most importantly supports "on demand" fabrication of various tissue compositions. This advanced 3D bioprinting technology, together with our mechanistic-based tissue engineering design principles, is expected to support customized design and fabrication of complex and scalable tissues for both research and medical applications.

CHAPTER 1. INTRODUCTION

Objectives

What is the long-term goal?

The goal of this research was to develop a prototype three-dimensional (3D) bioprinter fluidic mixing nozzle that accommodates i) standardized self-assembling collagens; and ii) facilitates on demand fabrication of tissue constructs with a wide range of cell and matrix compositions, including gradients. Based on this engineering design problem, the specific aims of this project were:

1. Design, build, and validate a prototype 3D bioprinting nozzle that accommodates self-assembling oligomeric type I collagen as the primary extracellular matrix (ECM) component, as well as cells. Nozzle performance will be characterized and validated in terms of i) dispensing accuracy over a range of volumes, flow rates, and syringe sizes; ii) mixing quality; and iii) maintenance of functional characteristics of delivered materials (i.e., structural-mechanical properties of deposited self-assembled collagen and cell viability).
2. Demonstrate the ability of the prototype nozzle to fabricate a collagen fibril density gradient.

This work represents significant progress in the area of 3D bioprinting for two reasons. First, self-assembling oligomeric type I collagen, is ideally suited for tissue fabrication, compared to currently used biomaterials, since it facilitates encapsulation of cells within collagen-fibril microenvironments that more closely resemble those found in native tissue

Second, the proposed design supports on demand dispensing of a broad range of cell and/or matrix composition and gradients from a single nozzle within the same tissue construct. This is an improvement over conventional bioprinter designs, which accommodate multiple reservoirs with a one-nozzle-one composition dispensing capacity.

Background

3D bioprinting has evolved from a field of science fiction, to a practical field with potential applications in wound care, *in vitro* pharmaceutical and chemical testing, and organ transplantation (Murphy 2014). Bioprinting was first defined in 2004 at an international workshop as “the use of material transfer processes for patterning and assembling biologically relevant materials–molecules, cells, tissues, and biodegradable biomaterials– with a prescribed organization to accomplish one or more biological functions” (Mironov 2006). More specifically, the goal of 3D bioprinting is re-create multicellular tissues and organs *de novo* (Mironov 2006). To date, great strides have been made to achieve this goal; such as the creation of tissue with pre-made channels for blood vessel attachment and human-scale, mechanically stable implants such as calvarial bone, cartilage and skeletal muscle (Zhang 2013, Kang 2016). These implants, while still in the realm of research in academia, provide visibility to what might be possible in future years for industry.

These 3D bioprinted tissues, or “tissue constructs”, are becoming more common with increased knowledge and accomplishments in the 3D tissue culture field. The field of 3D tissue culture is also expanding due to its improved physiologic relevance over conventional 2D cell culture (Rimann 2012). This shift from 2D to 3D tissue culture has brought to light the importance of the ECM. Specifically, how matrix stiffness, architecture, and ligand presentation affects cells. In turn, this has increased the need for scientists to systematically control and vary the properties of the ECM to induce a desired cell behavior (Mason 2013). As an additive manufacturing method, 3D bioprinting shows significant

potential to address these fabrication needs for advanced design and construction of complex and scalable living tissues.

Types of 3D Bioprinters

At present, there are three categories of 3D bioprinters, including inkjet, laser induced forward transfer (LIFT), and microextrusion (Murphy 2014). Each of these has its own advantages and disadvantages that make it well suited for different bioprinting applications in tissue engineering.

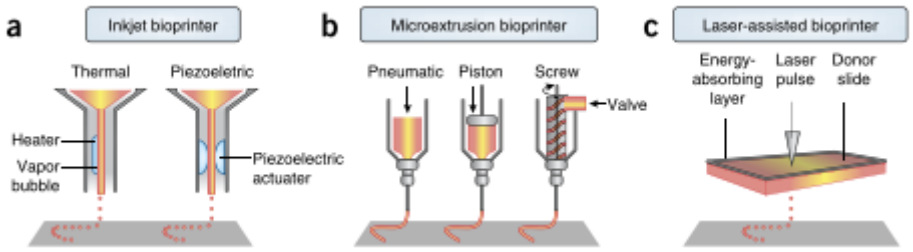

Figure 1. The three different types of bioprinters currently used for 3D bioprinting. (a) Inkjet bioprinters. (b) Microextrusion bioprinters. (c) Laser-Assisted Bioprinters. (Murphy 2014).

Inkjet Bioprinting

Inkjet bioprinters are very common; partly because in the early days of 3D bioprinting, you could very easily modify commercially available inkjet printers to print cells (Murphy 2014). The inkjet nozzle is used to place precise volumes of cells suspended in a biomaterial that are stored in a modified ink cartridge, just like the commercial inkjet printers. This, coupled with control over the x, y and z-axis, makes it possible for researchers to print droplets on the scale of pico-liters, at speeds of up to 10,000 drops/second, to create layers of cells with very high resolution (Murphy 2014). Researchers now use mostly thermal (Cui 2012) or piezo (Saunders 2008) controlled nozzles to achieve these speeds and low volumes.

The advantages of this style of bioprinting is the high cell viability (>80%), and high resolution (Horváth 2015). The disadvantages include the high susceptibility of nozzle clogging during the print, and the low volume dispensed per second when compared to other bioprinters (Ozbolat 2013). Because these printers lack the ability to print milliliters of biomaterial per second, like microextrusion printers, they are not typically used to create large tissue constructs. However; these bioprinters have been used in applications such as the creation of skin and cartilage (Skardal 2012, Cui 2012), where the total volume of the tissue construct is low, and can be created by stacking two-dimensional sheets of patterned cells.

Laser Induced Forward Transfer Bioprinting (LIFT)

LIFT 3D bioprinters are similar to inkjet bioprinters, but were made to overcome nozzle clogging limitations (Duocastella 2007). The mechanism underlying LIFT is arguably the most complicated of the three types being addressed, but a brief summary should aid in understanding the advantages of this type of bioprinter.

LIFT requires three components: a laser, a ribbon, and a substrate (Guillotin 2010). The ribbon is composed of a thin, transparent material, such as quartz or glass, which has a thin film of metal such as gold or titanium coated on one side. A thin layer of the biomaterial with encapsulated cells is applied to the metal film, and this whole component is flipped upside-down so the cells are facing down, and the side of the transparent material without a metal coating is facing upwards. A pulsing laser is then directed onto the top side of the thin metal layer, through the transparent material. The laser heats the metal to a plasma state, and this causes a shockwave that expels the biomaterial directly under the laser. The expelled biomaterial lands on the receptor substrate, which varies depending on the study, but can be as simple as a glass slide for imaging purposes (Guillemot 2010, Guillotin 2010).

Surprisingly, the heating of metal to a plasma state has very little effect on the cells or proteins (Guillotin 2010). LIFT bioprinters have cell viabilities on par or exceeding that of inkjet bioprinters, often above 90% (Murphy 2014), and do not suffer from clogging like inkjet bioprinters. LIFT bioprinters also operate at speeds which are very comparable to inkjet bioprinters (Mézel 2010). The droplets can be small enough to contain only one encapsulated cell (Duocastella 2007) or up to 5-7 encapsulated cells (Guillemot 2010). The issue with these small droplet sizes is that when the droplets are patterned in an array of individual droplets, they will evaporate. This challenge is overcome by the addition of glycerol to many LIFT biomaterials. However, if the glycerol content exceeds 10% v/v, it will compromise cell viability (Guillemot 2010). Another limitation of this type of bioprinter is the inability to print large-scale tissue constructs, much like inkjet bioprinters. LIFT has been used to create smaller tissue constructs (on the order of mm) such as cardiac patches that were later implanted into mice suffering from myocardial infarction (Gaebel 2011), and used extensively to create two-dimensional cell patterns (Guillemot 2010, Guillotin 2010, Duocastella 2007).

Microextrusion Bioprinting

The main type of 3D bioprinter that will be focused on in this work is microextrusion. The basis of microextrusion bioprinting is the same as extrusion-deposition 3D printers that have become popular with hobbyists and professionals (Ozbolat 2016). The main difference is instead of depositing plastic, the printer deposits a biocompatible material capable of cell encapsulation.

Most microextrusion bioprinters work by holding the ECM biomaterial in a reservoir in its liquid state. As such, biomaterials that undergo self-assembly, or a fluid to gel transition are utilized. Pressure is applied to the reservoir, by either pneumatic or mechanical-driven systems, which causes the biomaterial to flow

out of the reservoir and through an extrusion nozzle (usually outfitted with a syringe needle), as shown in Figure 1b. The nozzle deposits the biomaterial on the stage, where it is then converted into its gel-like state, most commonly done by means of photopolymerization (Kolesky 2014) or addition of an ionic crosslinking solution (Ozbolat 2014). An x-y-z robotic gantry system positions the extrusion nozzle over a platform where the tissue construct is created, point-by-point or layer-by-layer.

Modifications to this design have resulted in 3D bioprinters with multiple reservoirs and extrusion nozzles (Duan 2013, Smith 2004, Skardal 2010, Schuurman 2010, Wüst 2010, Pati 2014), and specialized nozzles to create complex geometries (Zhang 2013, 2015), shown in Figures 2a and 2b, respectively. Advantages of this bioprinter technology include i) the ability to print in high cell densities, ii) the ability to print large tissue constructs with moderate complexity, and iii) ease of use. The disadvantages are decreased cell viability, thought to be caused by the shear forces exerted on the cells in a viscous fluid, compared to the other types of 3D bioprinting, and decreased resolution (Ozbolat 2013). Arguably the most impressive tissue constructs have come from microextrusion bioprinters, such as the creation of human-scale, implantable tissues, such as calvarial bone, that show new blood vessel formation and host tissue integration 5 months after implantation (Kang 2016).

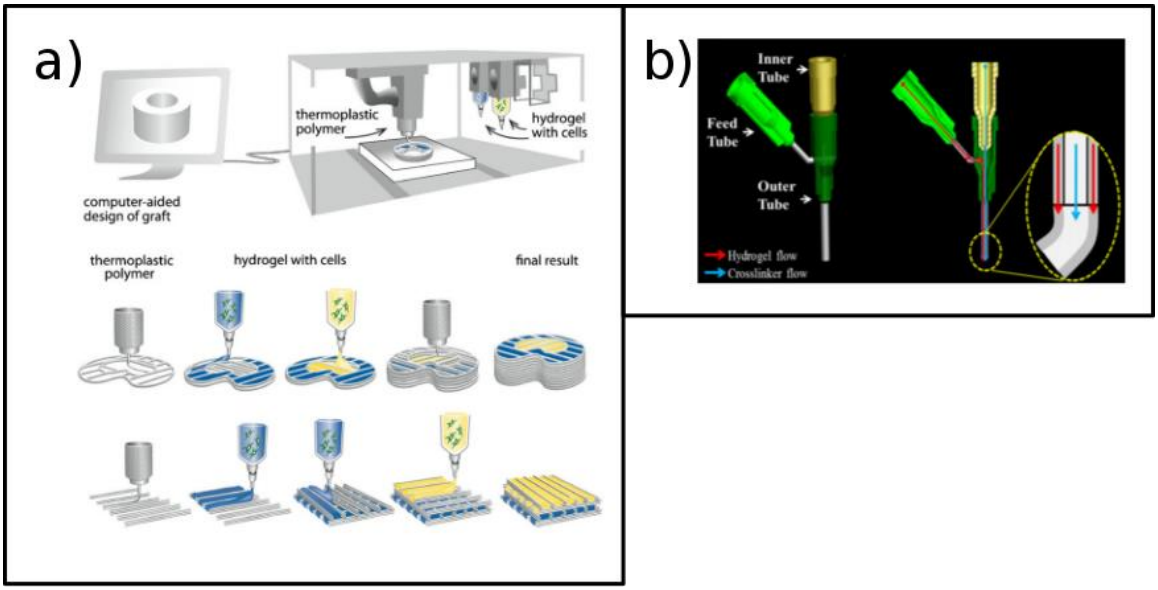

Figure 2. Modifications made to conventional microextrusion bioprinters that a) add the ability to print more than one bio-ink, and type of bio-ink, and b) allow for the printing of hollow hydrogel tubes (Schuurman 2011, adapted from Zhang 2013).

Table 1. Summary of the main features of each type of bioprinter (Murphy 2014).

Type of Bioprinter	Resolution	Cell Viability	Printed Cell Densities	Applications
Inkjet	μm	>85%%	$<10^6$	Thin layer tissue replacement and patches
LIFT	μm	>95%	$<10^8$	Thin layer tissue replacement and patches
Microextrusion	mm	40-80%	High	Human-scale tissue replacement

Bottom-up Versus Top-down Tissue Fabrication

These three types of bioprinters use two distinct methods to create tissue constructs: top-down and bottom-up. Both inkjet and LIFT bioprinting use the

bottom-up approach to create tissue constructs. This approach aims to mimic the heterogeneity of the cells, matrix, and growth factors of *in vivo* tissues with high spatial resolution (up to 1μm) printing of these components (Guillotin 2010). Using this method, researchers can attempt to mimic the organization and spatial distributions of various cell population, matrix components, and growth factor within a tissue, with the hope that the engineered tissue construct will function similarly to the target tissue. Using this method, researchers have been able to deposit droplets of biomaterial encapsulated cells (1-10 cells/droplet) with micron precision to create complex patterns, as demonstrated in Figure 3.

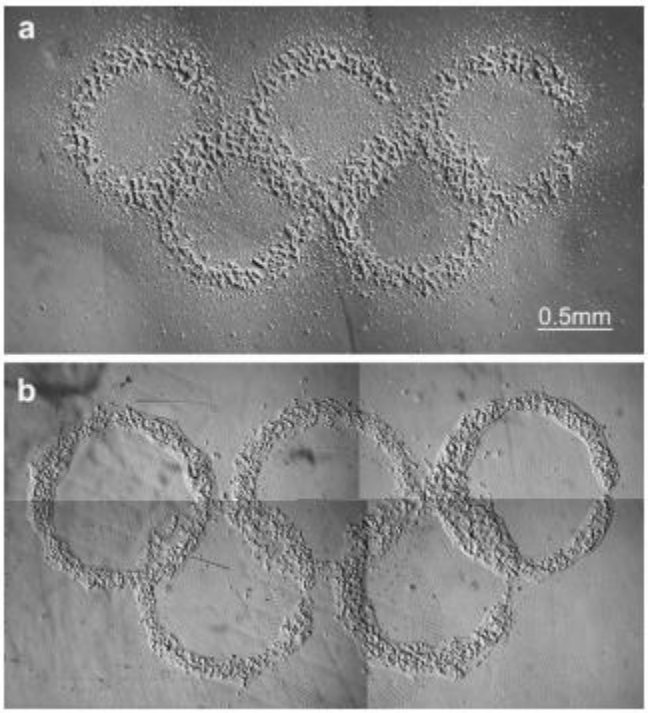

Figure 3. The precise deposition of cells in a specific pattern using the high resolution capacity of a LIFT bioprinter a) before the addition of 1% w/v alginate, and b) after the addition of alginate (Guillotin 2010).

In contrast, microextrusion bioprinting works by using the top-down approach. Microextrusion bioprinters do not have as high of resolution as LIFT or inkjet bioprinters, so they are unable to deposit cells and growth factors with the same spatial control as the bottom-up bioprinters. Instead, they recapitulate the

general shape and bulk mechanical properties of the tissue (such as stiffness), and deposit fewer cell types that have the potential to later differentiate and proliferate into a more heterogeneous cell population that more closely resembles native tissue. (Ozbolat 2014). This method relies on having a microenvironment that the cells can remodel, and a biomaterial that has the mechanical properties that allow it to hold its shape. With this method, researchers have been able to create tissue constructs that closely mimic the shape and structure of complex tissues, as shown in Figure 4.

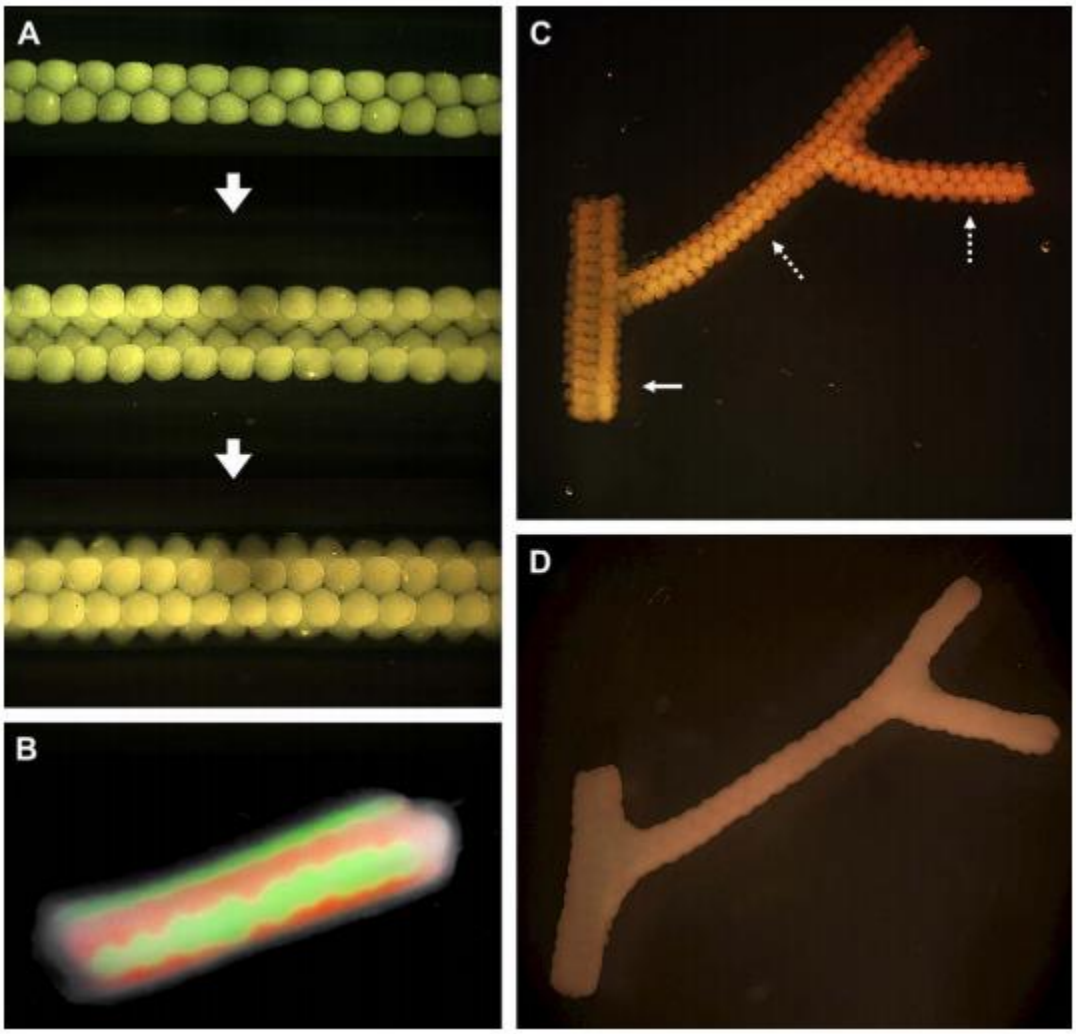

Figure 4. The deposition of individual high density cell spheroids to form a hollow, branched tube (Norotte 2009).

Gap in current 3D bioprinters

One gap in current microextrusion bioprinters is the inability to print heterogeneous tissue constructs, that is tissues containing various cells and/or matrix densities. The more complex microextrusion bioprinters have multiple reservoirs for different cell types and different materials, but the density (or concentration) of the biomaterial in all of the reservoirs is kept constant. As a result, these bioprinters are unable to achieve continuous gradients in cellular and/or matrix components as is found within natural tissues (e.g., skin, cartilage) *in vivo*. Therefore, the need exists for a bioprinter that allows the user to control and change the density of the matrix and/or cells within the same tissue construct. This new level of control will allow for more complex tissue constructs to be created, and more research to be done on the effects of heterogeneous ECM concentration and stiffness within tissue.

Biomaterial properties

While each bioprinter type uses specific biomaterials and biomaterial formats as their bio-ink, all biomaterials must fulfill three design criteria; i) biocompatibility, ii) printability, and iii) physiologic relevance.

One main design criterion for 3D bioprinter biomaterials is biocompatibility. The material that is printed will eventually serve as the ECM for the encapsulated cells. Therefore, the cells must be able to survive and execute fundamental behaviors, including proliferation, migration, differentiation, and morphogenesis. When thinking about biocompatibility, it is also important to know if and how the biomaterial will degrade. Biomaterial degradation mechanisms (cell-induced, proteolytic degradation or hydrolysis), byproducts produced, and how to control the degradation rate are all important considerations (Murphy 2014). Degradation of the biomaterial and deposition of ECM by resident cells affects the mechanical

properties of the scaffold and some degradation products have been shown to decrease cell viability (Hourd 2015, Lee 2016).

The second biomaterial design criterion is printability. Viscosity and curing-time are the primary factors that determine printability. The material must be viscous enough to hold its shape until the material converts into a more gel-like state, or polymerizes. This polymerization can take anywhere from a few seconds to a few minutes and is known as gelation-time (Murphy 2013). Many materials do not initially have favorable printing properties, but in order to be used for 3D bioprinting applications, they are modified with exogenous crosslinking agents for photo-polymerization, chemical polymerization, or ion-polymerization (Suri 2011, Rutz 2015, Rodrigues 2012).

The final biomaterial property that must be considered is physiologic relevance. Physiologic relevance describes the similarities of the biomaterial to the native ECM within the tissue of interest. It is not enough for the cells to survive in the biomaterial (biocompatibility). For the true potential of the cells to be realized, they must be able to proliferate, migrate, differentiate, and remodel the environment around them, as they would *in vivo*. Properties of physiologic relevance include the presence of ligands that would normally be found *in vivo*, a chemical structure of the biomaterial that closely resembles native tissue, and matching stiffness and concentration of the native ECM. All of the current biomaterials used in 3D bioprinting are evaluated against these three criteria.

Current biomaterials used in 3D bioprinting

Biomaterials used in 3D bioprinting can be divided into two categories: synthetic or naturally-derived polymers (Murphy 2014).

Synthetic polymers are any polymeric biomaterial that is man-made. The advantage of synthetic polymers is the ability to tune the chemical properties for a specific application. Properties like mechanical stiffness, degradation rate, and

porosity can all be controlled for the experiment (Kolesky 2014). The disadvantages of synthetic polymers is the lack of physiologically-relevant architecture and biological signaling capacity. For this reason, synthetic polymers are often used in conjunction with naturally-derived polymers or functional motifs (e.g., cellular binding domains) derived from these polymers. The naturally-derived polymer contains the cells, and is printed around a scaffold of synthetic polymer that provides mechanical integrity. Examples of popular synthetic biomaterials include polyethylene glycol (PEG), polycaprolactone (PCL), and pluronic F127.

Naturally-derived biomaterials are derived from a natural source. Naturally-derived biomaterials encompass both nature-derived and tissue-derived biomaterials. Tissue-derived biomaterials are specifically derived from animal tissue. The advantage of tissue-derived polymers is their biocompatibility and physiologic relevance. In 3D bioprinting, these biomaterials are often used to encapsulate cells. The disadvantages of these polymers include high lot-to-lot variation, poor mechanical integrity and lack of tunability. Properties like stiffness, porosity, degradation rate, and curing-time have historically not been controlled or characterized, leading to poor reproducibility within and between laboratories. To combat this, synthetic polymers are often used in the same tissue construct, as previously stated. Nature-derived biomaterials are derived from materials found in nature, but not animal tissue. These biomaterials often have similar biocompatibility characteristics to tissue-derived biomaterials, but lack physiologic relevance. Of the numerous nature-derived polymers used in 3D bioprinting, there are three that make up the majority: sodium alginate, gelatin methacrylate (GelMA), and type I collagen (Ozbolat 2016).

Sodium Alginate

Sodium alginate is arguably the most common biomaterial due to its wide availability, mechanical properties, and favorable gelation properties. Sodium

alginate is a nature-derived block copolymer that is typically harvested from brown seaweed, and is composed of different ratios of two monomers: guluronic acid and mannuronic acid, or G units and M units, respectively (Rowley 1999). Two molecules of alginate bind together between G units when a di-valent or tri-valent metal ion bonds to one strand of alginate, and a separate strand also binds to the same ion, as shown in Figure 5. The resulting structure entraps the ions similar to eggs in a carton, which results in the name “egg box” model (Sachan 2009). The addition of these ions causes alginate to form a gel, and the ability of alginate to undergo gelation with only the addition of ions, like Ca^{2+}, as well as rapid gelation time, makes it an attractive biomaterial to use for bioprinting (Murphy 2013). However, because alginate is not found naturally in the body, this biomaterial lacks the inherent biological signaling capacity found in biomaterials derived from animal tissue. This means mammalian cells are unable to degrade and modify the alginate because they lack the enzymes to cleave the polymer chain (Lee 2012). Mammalian cells are also unable to interact with alginate gels due to the discouragement of protein adsorption by the hydrophilic nature of alginate (Rowley 1999).

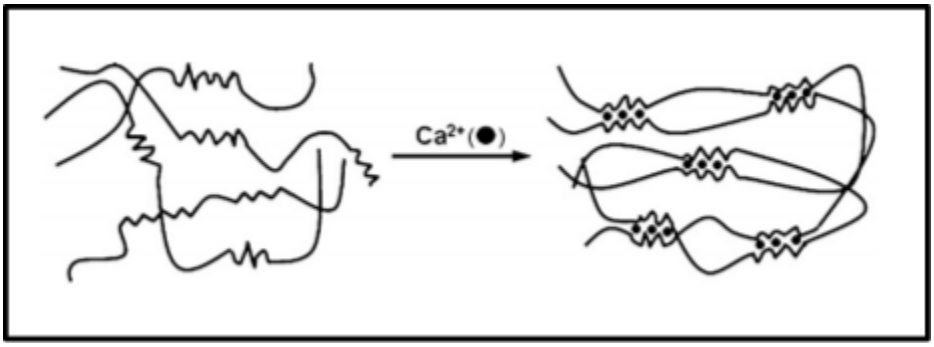

Figure 5. Molecules of alginate being bound together in an “egg box” formation by the addition of sodium ions (Lee 2012).

GelMA

Gelatin methacrylate is a very popular biomaterial that is advantageous for its photo-polymerization and a microstructure that is more physiologically relevant

than non-tissue derived biomaterials, such as alginate (Skardal 2014). Gelatin is derived from the partial hydrolysis of collagen, the most abundant protein in the ECM of animals (Gómez-Guillén 2011, Stenzel 1974). The partial hydrolysis of collagen breaks down the triple helix molecular structure, but keeps many of the arginine-glycine-aspartic acid sequences (RGDs) that promote cell attachment *in vivo*. The hydrolysis also does not affect the regions of the protein that are susceptible to degradation by matrix metalloproteinases (MMPs); the enzyme used by mammalian cells to degrade and remodel the local ECM (Yue 2015). When gelatin is cooled, there is an incomplete regain of the triple helix structure, and the gelatin solidifies (Van Den Bulcke 2000). This leads to a biomaterial with much greater physiologic relevance than synthetic or non-animal derived biomaterials.

One of the major disadvantages with this material is its gelation. Polymerization of gelatin without any additives is thermally reversible, and gels will revert back to a liquid state at physiologic temperatures. One of the more popular ways to stabilize the gel is to add methacrylic anhydride (MA), which binds to the amine and hydroxyl groups of the gelatin, and causes the permanent gelation of the combined materials (GelMA) upon exposure to UV light (Yue 2015), and in presence of a photoinitiator, as illustrated in Figure 6. The addition of MA only affects 5% of the amino acid residues in molar ratio (a degree of substitution, DS, of 5%), so it is thought that the vast majority of RGDs are still available to interact with the cell (Van Den Bulcke 2000). Because of its photo-polymerization capacity, GelMA has been used extensively to create very complex and very small shapes that are much more easily made via the precise application of UV light (Gauvin 2012).

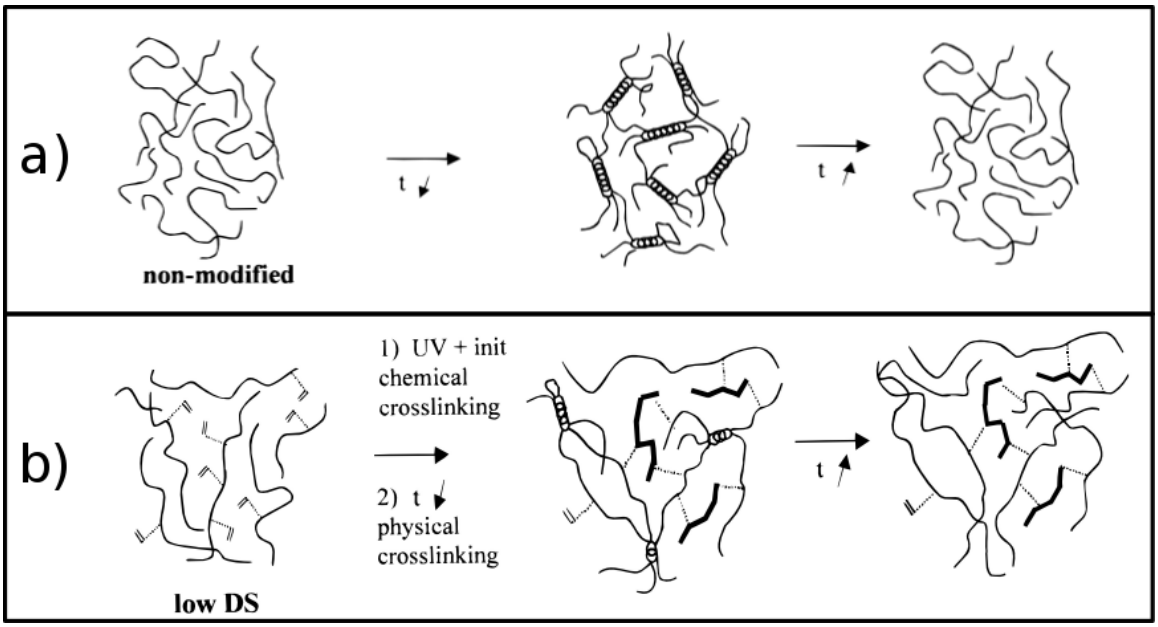

Figure 6. The polymerization of a) pure gelatin into helical structures, when temperature (t) decreases, and subsequent dissociation when the temperature is increased; and b) the polymerization of GelMA with a low degree of substitution (DS) in presence of UV light, photoinitiator and decreased temperature, resulting in both helical bonds and chemical crosslinks, and subsequent dissolution of the helical bonds upon heating (adapted from Van Den Bulcke 2000).

Collagen Type I

Type I collagen is an abundantly used biomaterial in 3D bioprinting because of its physiologic relevance and its ability to self-assemble *in vitro* and *in vivo* (Murphy 2013). The fundamental building block of collagen is tropocollagen, or telocollagen, and consists of a triple helical structure, capped by short telopeptide regions. These telopeptide regions participate in the self-assembly of tropocollagen into microfibrils, which further assemble into fibrils in a fibrillar matrix structure (Bailey 2011).

Monomeric collagen formulations, telocollagen and atelocollagen, have traditionally been used as biomaterials for 3D bioprinting. However, these formulations have been shown to suffer from variable purity and poor self-assembly capacity (Abraham 2008). Upon neutralization to physiologic pH and ionic strength, monomeric collagen solutions self-assemble at the fibril level into

entangled individual fibrils, as shown in Figure 7a, and because of the lack of suprafibrilar assembly, the resulting matrix often suffers from poor mechanical integrity and shape definition (Blum 2016). For monomeric collagen, gelation is induced by increasing the temperature of neutralized solutions to physiologic temperatures. This makes them an attractive biomaterial for the sake of simplicity, but this polymerization process takes longer (typically 30 minutes or greater) than many other biomaterials used in bioprinting. To compensate, another biomaterial is often used to help collagen retain its shape (Chang 2011). The benefit of monomeric collagen is that it self-assembles into a fibril format, providing superior physiologic relevance when compared to almost all other biomaterials. However; even though this biomaterial is more physiologically relevant than many other popular biomaterials used in 3D bioprinting, there is still a need for a better biomaterial.

Oligomeric collagen formulations are comprised of molecular aggregates of telocollagen molecules (e.g., trimer) that uniquely retain their natural intermolecular crosslinks (Bailey 2011). Compared to conventional collagen monomers, oligomers exhibit more robust, rapid, and superior fibril-matrix assembly, yielding highly interconnected collagen-fibril materials (Kreger et al. 2010, Bailey et al. 2011). Because oligomers exhibit both fibrillar and suprafibrillar assembly, they support user customization and tunability across the broadest range of fibril architectures and mechanical properties. Tuning fibril density is achievable by controlling collagen concentration, as they are directly related (Kreger et al. 2010). As shown in Figure 7b, the structure resulting from the self-assembly of these molecules leads to matrices with suprafibrillar and fibrillary organization. This, in turn, leads to decreased gelation time, increased physiologic relevance, increased mechanical properties, and increased tunability when compared to monomeric collagen. Oligomeric collagen is the only formulation that is standardized (ASTM Standard F3089-14) and quality controlled based upon its molecular composition and polymerization capacity, providing the necessary reliability and reproducibility for 3D printing (ASTM

F3089-14 2014).

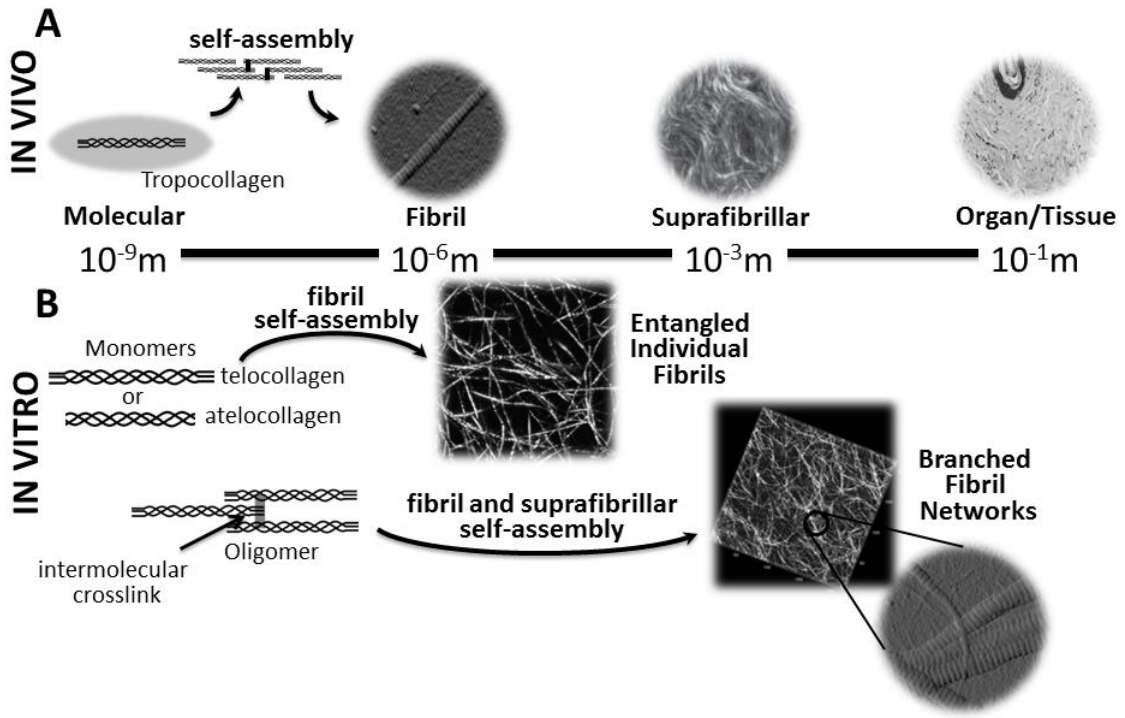

Figure 7. Summary of the assembly of monomeric and oligomeric type I collagen both *in vivo* and *in vitro* into fibril matrices (Blum 2016).

Gap in current biomaterials

There is one property of biomaterials used in 3D bioprinting that is consistently overlooked: physiological relevance. Although type I collagen is the most physiologically relevant biomaterial, as it is the most abundant protein in the ECM of humans (Stenzel 1974), many 3D bioprinters modify its chemistry for better printability or mechanical integrity. This is because most collagen used in 3D bioprinting is poorly characterized, has uncontrollable gelling, and has poor mechanical integrity (Jang 2016). What is needed is a type I collagen biomaterial that is well characterized and mechanically stable, and a 3D bioprinter that is able to take advantage of the superior tunability of this biomaterial.

Being able to easily modify the mechanical properties of a highly

physiologically-relevant biomaterial, without the addition of exogenous chemicals, would allow researchers to study tissue constructs that more closely recapitulate the native *in vivo* tissue.

Recapitulation of Tissue and Organ Heterogeneity

All tissues are composed of cells and an ECM, organized to address specific structural and functional demands of the tissue. Not only does tissue function vary widely within the body, it also varies widely within tissues and organs themselves. Because of this heterogeneity within tissues, complex architectures such as gradients of cellular and ECM components are often found *in vivo*.

ECM stiffness and concentration differ greatly in the body (Justin 2011); not only between different types of tissue, but also within tissues themselves (Wells 2008). For instance, the stiffness of brain tissue is around several hundred pascals (Pa), but the stiffness of muscle is more than 12 Kilopascals (kPa), and the stiffness in the liver alone can range from 300 to 600 Pa in healthy tissue, and up to 20 kPa in diseased tissue (Wells 2008). Continuous ECM stiffness gradients are also found in the body, such as in the ligament-to-bone interface, as shown in Figure 8, and in the deeper layers of skin (Justin 2011). This knowledge has led to studies on the effect of ECM concentration, and stiffness gradients in particular, on various cell types.

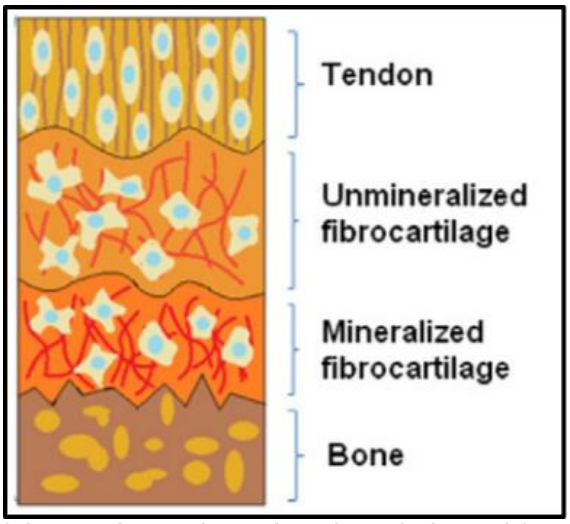

Figure 8. Schematic of the tendon-to-bone interface (adapted from Seidi 2011).

The fact that ECM stiffness gradients affect cell function has been well established (Shamloo 2010). Cells sense the change in ECM stiffness with surface receptors known as integrins (Friedl 1998). Integrins on the surface of cells bind to ligands in the ECM in order to move the cell during migration. The activation of these receptors causes the regulation of many different pathways within the cell, which cause various cell behaviors such as cell migration (Georges 2005). However, many studies regarding the effect of ECM stiffness on cell behavior have been done in 2D. This has been done to extricate confounding variables that accompany increasing the stiffness of a 3D matrix, such as decreased porosity and an increase in the number of ligand-adhesion points for cells (Georges 2005). Considering the primary goal of these studies has been to characterize the effect of ECM stiffness alone, removing confounding variables is to be expected. These studies have also been performed exclusively in 2D due to the lack of well characterized and tunable biomaterials that can be used for 3D cell studies (Mason 2013, Gu 2016).

From 2D studies, ECM substrate stiffness has been shown to play a major role in development (Justin 2011), cancer progression (Lu 2012), disease progression (Wells 2008), neuron function (Balgude 2001), and stem cell

differentiation (Justin 2011). While these studies show a clear effect of the substrate stiffness on different cell functions, it is well known that the results might not translate when performed in a 3D environment. Doing experiments such as these in 3D matrices that are physiologically relevant is important to increasing our understanding of how ECM concentration and stiffness affects cells *in vivo*.

Fortunately, there have been *in vitro* studies in 3D cell cultures that prove that ECM stiffness and concentration have similar effects on cells. For instance, in the area of vasculogenesis, varying ECM stiffness causes morphological changes in the resulting vascular network (Whittington 2013). Unlike 2D studies, 3D experiments are often not able to remove the confounding variables such as variable ligand density, but they more closely recapitulate the *in vivo* cellular microenvironment (Hadjipanayi 2009). A further benefit of performing ECM concentration and stiffness experiments in 3D matrices is allowing users to observe cellular phenomenon that only happen naturally in 3D, such as the formation of a vacuole in vasculogenesis or angiogenesis.

It is clear that in order to have tissue constructs that recapitulate the ECM found *in vivo*, there must be a focus on matching the heterogeneity of native ECM concentration and stiffness. That is why I have proposed a novel 3D bioprinting nozzle to address this issue.

Proposed 3D Bioprinter

The bioprinting nozzle was designed to accomplish the following goals:

1. Combine and mix the three reagents of oligomer, diluent, and S.A.R continuously, over the course of printing the tissue construct.
2. Control the temperature of the fluids inside the nozzle
3. Print a wide range of collagen concentration from only the three stock reagents, all within the same tissue construct.

If the bioprinting nozzle accomplished all of these goals, it would be the first 3D bioprinter to use oligomeric type I collagen, and the first bioprinter to print a tissue construct with a heterogeneous ECM concentration from a single biomaterial. Not only would the system be able to print multiple concentrations of collagen, and therefore different fibril densities, but it would be able to print a broad range of concentrations, in a linear gradient.

CHAPTER 2. MATERIALS AND METHODS

Design of the 3D Bioprinting Nozzle

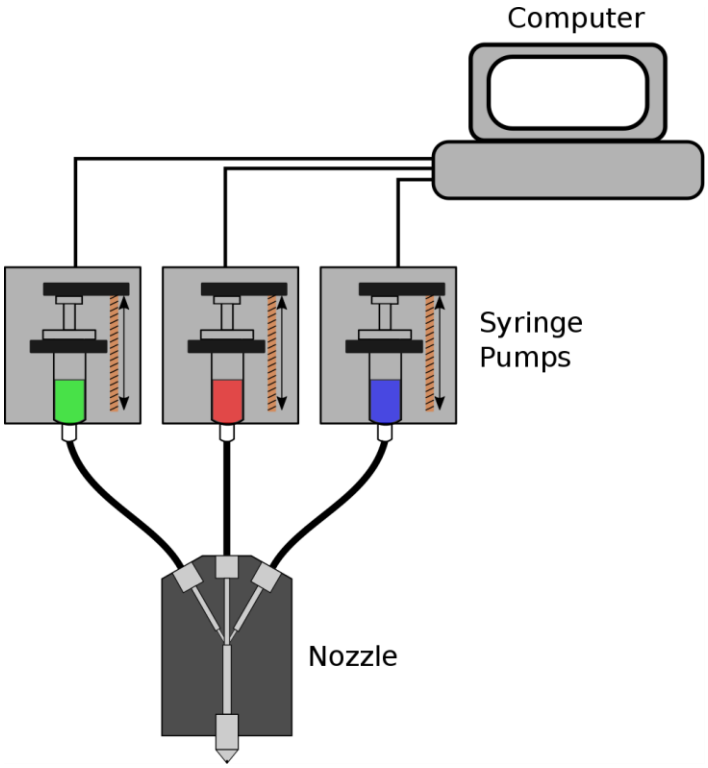

Figure 9. Complete system diagram.

Design of the complete bioprinting nozzle, as shown in Figure 9, was broken into four steps:

1. Chamber design, modeling, and fabrication
2. Solution dispensing
3. Graphical User Interface (GUI) development

4. Evaluation and optimization of nozzle for printing self-assembling collagen

Type I Oligomeric Collagen Preparation

Type I oligomeric collagen was acid-solubilized from the dermis of market weight pigs and lyophilized for storage as described previously (Bailey 2011). According to ASTM International standard F3089-14, the oligomeric formulation was standardized on the basis of polymerization capacity and molecular composition (ASTM F3089-14 2014). Polymerization capacity is defined by the shear storage modulus *G'*, in Pa, as a function of oligomer concentration.

Design, Computational Modeling, and Fabrication of Mixing Chamber

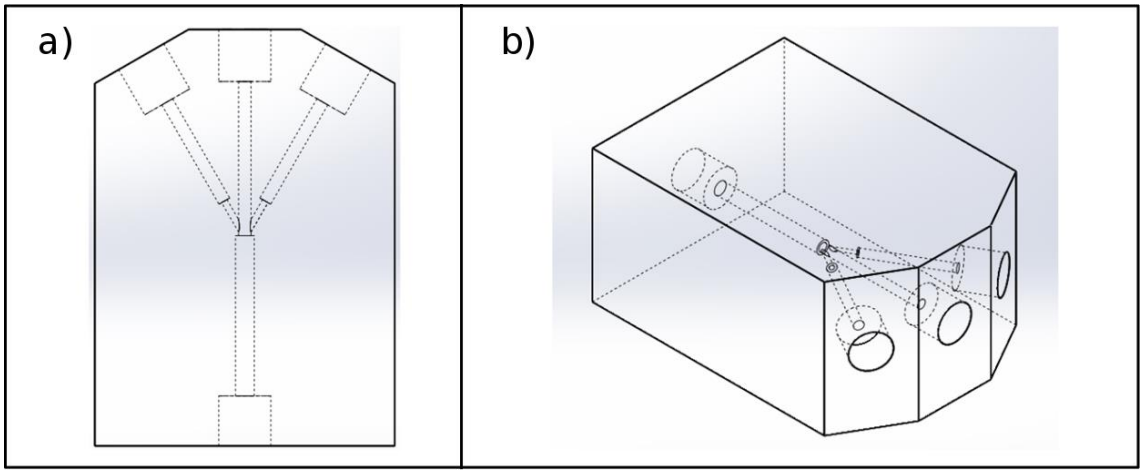

Figure 10. CAD drawings of the designed mixing manifold from a top-down view, a); and from an orthogonal view.

A mixing manifold was designed to achieve *continuous* mixing of three fundamental reagents, oligomer, diluent, and S.A.R, needed to produce self-assembling collagen-fibril matrices over a broad range of microstructure-mechanical properties, as shown in Figure 10. Other important design criteria

included biocompatibility, chemical resistance, sterilizability, and adequate thermal conductivity to facilitate temperature control.

The chamber was designed to include three channels (0.06” in diameter), with the two outer channels offset from the central channel by an angle of 30 degrees. The diameter of the two outer channels narrowed to 0.03” as the two outer channels intersected the central channel (Figure 11). According to Gobby and co-workers, this angle of 30 degrees supports optimal mixing efficiency for passive, microfluidic T-mixers (Gobby 2001). Narrowing of the outer two channels was done to increase the velocity of the two outer streams of fluid (Diluent and S.A.R) at the point of combination with the oligomer. Decreasing the diameter of channels induces a venturi effect on the fluids, which was shown to further increase the mixing efficiency in angled T-mixers (Gobby 2001). Holes for three, 1/4-28 barbed fittings were added to the nozzle at the end of each channel to allow for attachment of reagent lines.

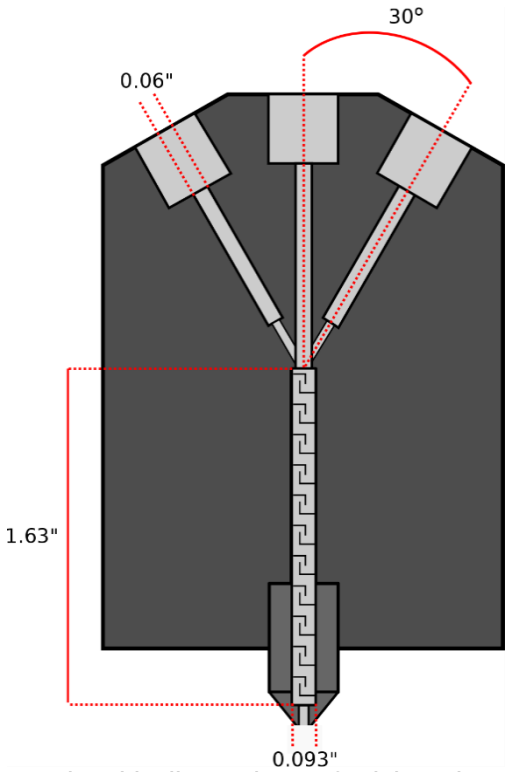

Figure 11. Schematic of the nozzle with dimensions of mixing chamber and channels for reference.

Immediately following the intersection of the three channels, a mixing chamber was added (0.093” in diameter) to ensure thorough mixture quality. To aid in this, a disposable static mixer was placed in the mixing chamber (Nordson EFD; East Providence, RI). Twisted channel mixing mechanisms induce complex fluid dynamics, and are commonly added in mixing applications to increase the mixing efficiency and mixture quality (Thakur 2003). For easy removal of the static mixer, the mixing chamber was not made to fully house the static mixer, as shown in Figure 12. The protruding end of the static mixer is housed in the needle.

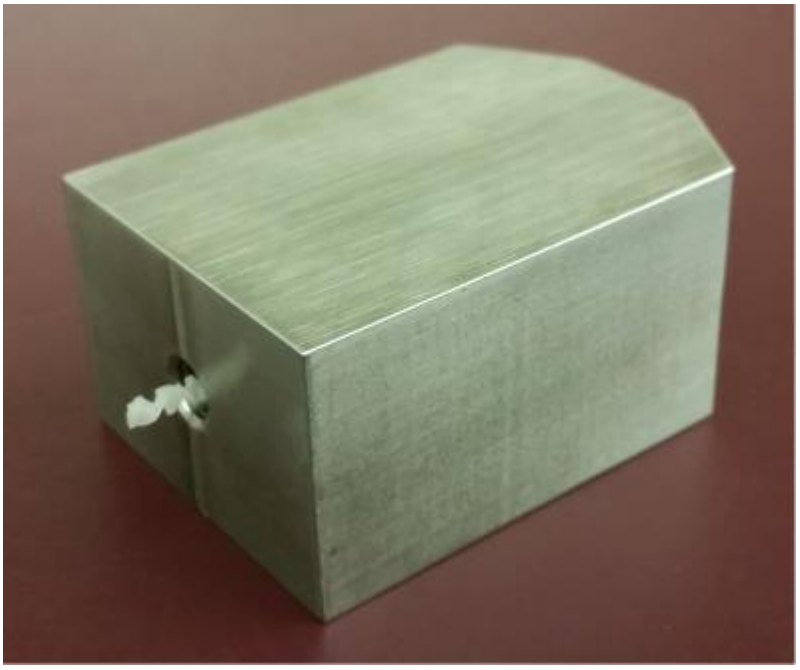

Figure 12. Protruding end of the static mixer before the needle has been screwed into place.

The needle was used to house the protruding end of the static mixer, and to direct the flow of neutralized collagen onto the substrate. To minimize the surface tension between the deposited collagen and the needle, the end of the needle was machined into a cone. A small hole was machined into the cone-shaped end (.0295” in diameter) to focus the deposition of collagen.

Computational Modeling

Computational modeling was performed to ascertain the value of narrowing the outer channels before they intersected at the inner channel. Two 2D models of the nozzle channels were constructed in a CAD program (Solidworks, Dassault Systems) and imported into COMSOL Multiphysics 5.2. One model did not have narrowed outer channels, and the other had channels narrowed to 0.03” in diameter, directly before the intersection of the three channels. Laminar flow

physics was selected, as initial calculations suggested the flow in the channels would not reach turbulent levels.

Reynolds number was calculated using the following formula for pipe flow:

$$\text{Reynolds Number} = \frac{QD}{\nu A}$$

Where Q is equal to the flow rate, D is equal to the diameter of the pipe (0.06” if not narrowed, and 0.03” if narrowed), ν is the kinematic viscosity, and A being equal to the pipe cross-sectional area.

Flow rates at each inlet to the three inlet channels were estimated from the conversion of expected 3D flow rates to 2D flow rates, and the average fluid velocity was measured at the entrance to the mixing chamber. The average fluid velocity was calculated by averaging the fluid flow velocity vectors along a horizontal line extending from one side of the entrance to the mixing chamber to the other. This vector was then converted into a magnitude and compared across other fluid simulations. This was done for both narrowed and unchanged diameter models. The materials in the models were varied between using water as all three reagents, and having water as the reagents in the outer two channels, and a material simulating the viscosity of the oligomer in the central channel. Percent increase in fluid velocity was calculated by comparing the average fluid velocities of two simulations using the same fluid and inlet conditions, but different channel geometry.

Nozzle Fabrication

Fabrication of the main body of the nozzle was done by a separate company (Wirecut Industries, Indianapolis, IN). The needle was fabricated in-house. Both the main body of the nozzle and needle were manufactured out of 304 stainless

steel. This metal exhibits acceptable biocompatibility properties, is autoclaveable, and has excellent thermal conductivity.

Solution Dispensing

To control the concentration of printed collagen, the ratio of the flow rates of oligomer and diluent were varied. Varying the ratio of flow rates of these two reagents changed the final concentration of the neutralized collagen. Control of solution dispensing was performed by three lead-screw driven syringe pumps (New Era Syringe NE-500, Farmingdale, NY), independently controlled by a GUI developed in-house.

GUI Development

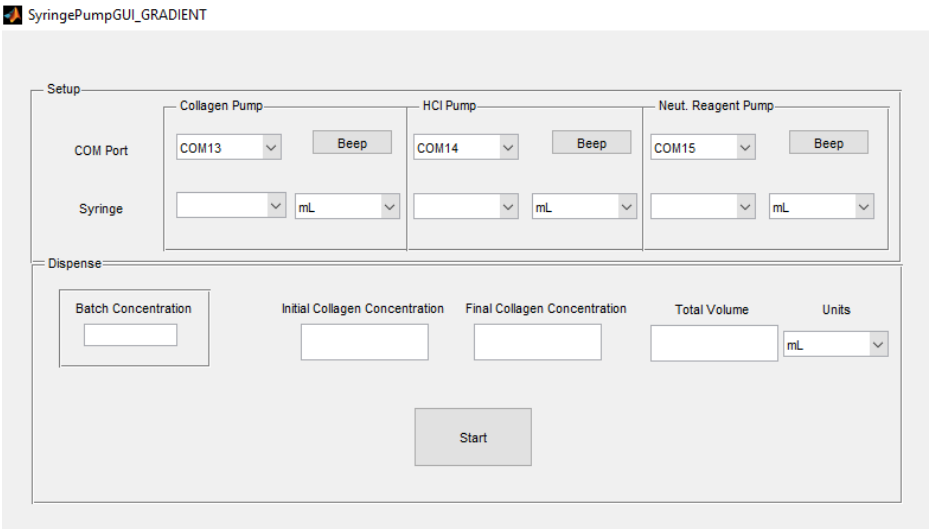

Figure 13. Screenshot of the GUI developed in-house, to control the 3D bioprinting system.

The GUI was developed in MATLAB (Mathworks, 2014), and the summarized process of the user input is explained below:

1. The user specifies which reagent is loaded in each syringe pump
2. The user selects what brand and size of syringe each reagent is in
3. The user inputs the collagen concentration of the oligomer
4. The user inputs the desired concentration of printed, neutralized collagen that is to be dispensed from the printer
    a. If the user requires a single concentration, input the same concentration for both the initial concentration and final concentration of printed collagen
    b. If the user requires a linear gradient of collagen concentration, input the desired initial concentration, and the final concentration of the printed collagen
5. The user selects the total volume of collagen to be dispensed from the nozzle

Evaluation and optimization of nozzle for printing self-assembling collagen

3D bioprinting nozzle performance was validated in terms of:

1. Separate reagent dispensed volume accuracy
2. Simultaneous reagent dispensed volume accuracy
3. Mixing quality
4. Viscoelastic properties of self-assembled collagen
5. Gradient formation
6. Cell viability

Separate reagent dispensed volume accuracy

Dispensed volume accuracy was measured using one syringe pump and dispensing either oligomer or water through the middle inlet channel or either of the side inlet channels, respectively. Water was used an analog for the diluent and the S.A.R, as their viscosities are similar.

Water was placed into a 10cc syringe (BD Biosciences; San Jose, CA) and secured into the syringe pump. The outlet of the syringe was attached to a side inlet port of the bioprinting nozzle using flexible tubing. Three samples of water (n=3) were dispensed (50, 100, 500, and 1000 uL) at each flow rate (10, 50 and 100 uL/sec) and weighed (Sartorius BP 210D; Goettingen, Germany). After completion, the 10cc syringe of water was replaced by a 20cc syringe of water, and the process was repeated. Once it had been repeated with the larger syringe, the entire experiment was conducted again with un-neutralized collagen attached to the middle inlet port of the nozzle.

Simultaneous reagent dispensed volume accuracy

Three different fluorescent dyes, Rhodamine 110 (Sigma, St. Louis, MO), Rhodamine 6G (Sigma), and Rhodamine B (Sigma) were added to the diluent (0.4 mg/ml), oligomer (0.4 mg/ml), and S.A.R (0.2 mg/ml), respectively. Hand-mixed and printed reagents were all made to achieve final neutralized collagen samples made from the dyed reagents. These samples were made at concentrations of 1.34, 1.92, 2.36, 2.73 and 3.06 mg/mL. Fluorescence of the hand-mixed and printed samples was measured in a spectroflourometer at excitation/emission wavelengths of 496/520, 526/555, and 550/625 for rhodamine 100, 6G and B, respectively (Spectramax i3x, Molecular Devices, Sunnyvale, CA).

Dispensed volume accuracy of each reagent was measured by comparing the fluorescence values of printed and hand-mixed samples for corresponding collagen concentrations. 400 µL of each concentration was hand-mixed using the dyed reagents, and from that, three, 100 µL samples were plated into three wells of a 96 well plate (Costar; Sigma), (n=3). For printed samples, 150 µL of each concentration was printed from the nozzle, into a 1.5 mL Eppendorf tube.100 µL of that was plated into a well of a 96 well plate. This process was repeated three times (n=3). After three samples of each concentration had been plated, the plate was placed in an incubator, held at 37 °C and 5% CO_2 for ten minutes to allow for complete polymerization of samples. This process was repeated three times (N=3). After the final incubation, the fluorescence of all samples was measured (Spectramax i3x; Molecular Devices, Sunnyvale, CA). Accuracy was determined using the formula:

$$Accuracy = \ 100 - \frac{|Accepted - Experimental|}{Accepted} * 100\%$$

Where the accepted value corresponded to the value of the hand-mixed samples and the experimental value corresponded to the value of the printed sample for each reagent.

Precision was calculated using the following equation:

$$Precision = \frac{|\mu - s_n|}{s_n} * 100\%$$

Where µ was the average fluorescent intensity for each reagent, and s_n was each individual fluorescent value.

Mixing Quality

Mixing quality is defined as the coefficient of variation (Statiflo 2016). As such, mixing quality was measured by the following formula:

$$\frac{Average}{Standard\ Deviation}$$

Where average was the mean of the nine fluorescent values of each reagent of both hand-mixed or printed samples, and similarly, the standard deviation of the nine fluorescent values.

Viscoelastic properties of self-assembled collagen

Batches of oligomeric collagen are subject to a quality control process, as defined by the ASTM standard guidance document (ASTM F3089–14 2014). In accordance with this document, quality control was done through rheometric testing of the polymerization capacity of the collagen. Three printed collagen samples were made at each of the aforementioned concentrations, and printed directly onto the rheometer base (AR2000; TA Instruments, Newcastle, DE), (n = 3) at volumes of 950 µL. These samples were compared to the standard curve of the batch of collagen the reagents were taken from, and their storage moduli were compared to three hand-mixed samples as the gold standard with a standard t-test analysis of means; significance was determined with $\alpha<0.05$.

Gradient Formation

A custom polymerization chamber was fabricated for the polymerization of 3 mLs of oligomeric collagen. The chamber was held under the nozzle and, as the nozzle dispensed 3 mL of collagen concentration starting at .5 mg/mL and ending at 4 mg/mL, was moved along its longer axis to facilitate gradient formation. Afterwards, the collagen was placed inside an incubator held at 37°C and 5% CO_2 for 30 minutes, and the resulting structure was imaged using confocal reflectance microscopy (Blum 2016). This imaging technique allowed the fibril

microstructure to be visualized, to qualitatively compare the relative fibril density of different locations along the length of the structure.

Cell Viability

Cell viability was measured using 0.4% trypan blue cell viability assay (Strober 2001). Neonatal human dermal fibroblasts (Lonza; Mapleton, IL) were cultured in Dulbecco's modified Eagle's Medium (DMEM; Sigma, St. Louis, MO) and supplemented with 10% fetal bovine serum (FBS, Sigma), 100U/ml penicillin (Gibco, Carlsbad, CA) and 100 µg/ml streptomycin (Gibco). Cells were maintained in a humidified environment of 5% CO_2 at 37°C over a period of two weeks, and split at 90% confluence. Cells suspended in DMEM were placed in a 3cc syringe at a concentration of $5x10^5$ cells/mL, and loaded into a syringe pump. The syringe was attached to a side channel of the bioprinting nozzle via a flexible rubber tube, and 500 uL of media and cells were deposited in a 48 well plate at varying flow rates (1000, 100 and 10 uL/sec). 500 uL of fibroblasts in media was taken from the stock solution, without being printed, for the negative control. This experiment was repeated three times (n=3), and the cell viability was recorded.

Statistical Analysis

All measurements are reported as mean ± standard deviation. Statistical analyses were performed with SAS v. 17 (SAS Institute, Cary, NC). To determine differences among treatment groups, the general linear model procedure (GLM) was used to conduct unbalanced analysis of variance (ANOVA) and perform multiple comparisons of least squares means using the Tukey-Kramer method. For simultaneous reagent dispensed volume accuracy analysis, a completely blocked three factor ANOVA was used to determine significant effects of syringe size, reagent viscosity, flow rate, total volume programmed to be dispensed, and their interactions ($\alpha = 0.05$) on the actual volume dispensed

by the nozzle. Differences were considered significantly different with the critical global p value of 0.05.

CHAPTER 3. RESULTS AND DISCUSSION

For the first step, it was necessary to quantitatively define mixing quality, as to have appropriate design criteria for the quality of the mixed reagents. Mixture quality was statistically defined as the mixture concentration's coefficient of variation (Vanarase 2010, Günther 2006, Dreher 2009). This can be thought of as how evenly distributed the fluids are in the mixture. This is typically measured by sampling the concentration of a dilute solution in multiple places in the container it is stored in, and calculating the standard deviation between the measured concentration values. A typical objective for high mixing quality is between 0.01 and 0.05, which ensures complete homogeneity of the mixture (Statiflo 2016).

Narrowing outer nozzle channels increased fluid velocity into the mixing chamber

Reynolds number calculations returned a maximum value of 2.7 for the narrowed channel design and 2.3 for the unchanged channel design at the inlet to the mixing chamber, indicating that the fluid would not be in the turbulent range. This initial finding prompted the need for additional mixing strategies and confirmed the use of laminar flow for the channel flow simulations.

Modeling nozzle channel geometry of both narrowed and unchanged channel diameters established that decreasing the outer channel diameter increased fluid velocity of fluid entering the mixing chamber. The effect of narrowing the channels can be seen visually in Figure 13, as the lighter color of fluid indicates a higher fluid velocity. The average percent increase in fluid

velocity between the narrowed channel design and unchanged channel design is shown in Table 2.

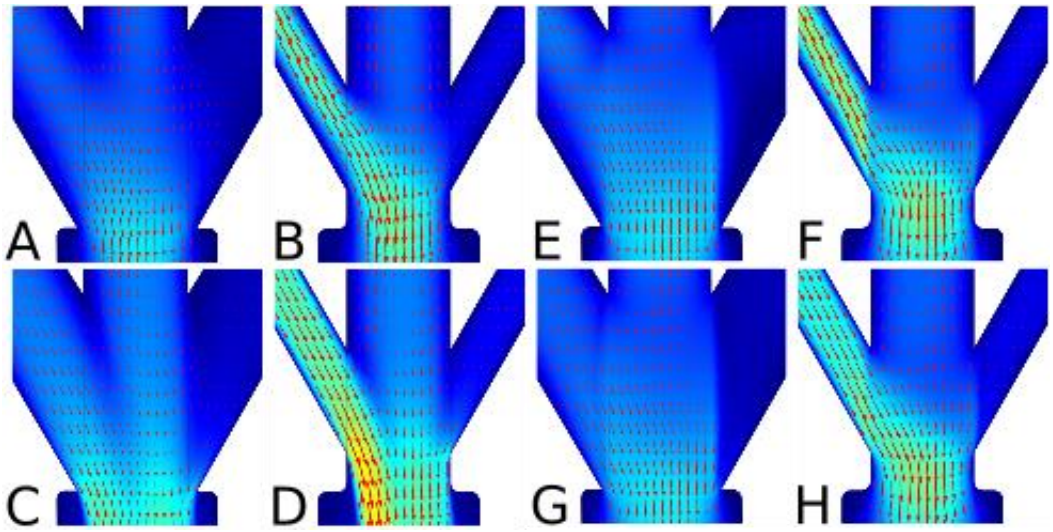

Figure 14. COMSOL models showing the effect of narrowing the outer channels on fluid velocity. Models were developed for A and B) Water flowing out of the nozzle at 10 µL/s, C and D) Water flowing at 100 µL/s, E and F) oligomer in the central channel with water in the outer channels at 10 µL/s, and G and H) oligomer in the central channel with water in the outer channels at 100 µL/s.

Table 2. Average percent increase in fluid velocity in narrowed channel design compared to unchanged channel design.

	Unchanged Channels		Narrowed Channels		Percent Increase (10 / 100) µL/s
Expected 3D Flow Rate at Outlet (µL/s)	10	100	10	100	
Water	0.004513	0.04510	0.00536	0.05438	18.8 / 20.6
Oligomer	0.004453	0.04466	0.005342	0.05339	20.0 / 19.5

This data demonstrated the utility of decreasing the diameter of the outer channels in order to increase the fluid velocity of fluid entering into the mixing

chamber. Increased fluid velocity is beneficial in this instance, due to its positive correlation with mixing quality (Gobby 2001).

Single reagent volume dispensing showed a significant flow rate and total volume interaction effect

Statistical analysis of dispensed volume accuracy showed no significant effect of changing the syringe volume size, but significant effect of the interaction between flow rate and volume dispensed ($\alpha = 0.05$), (Table 2). This significant interaction effect can be seen as a trend in the raw data of both water and oligomer for either syringe size (Figures 15a-15d). For the higher flow rates (500 and 1000 uL/sec), the accuracy of the dispensed volume is positively correlated with the expected dispensing volume.

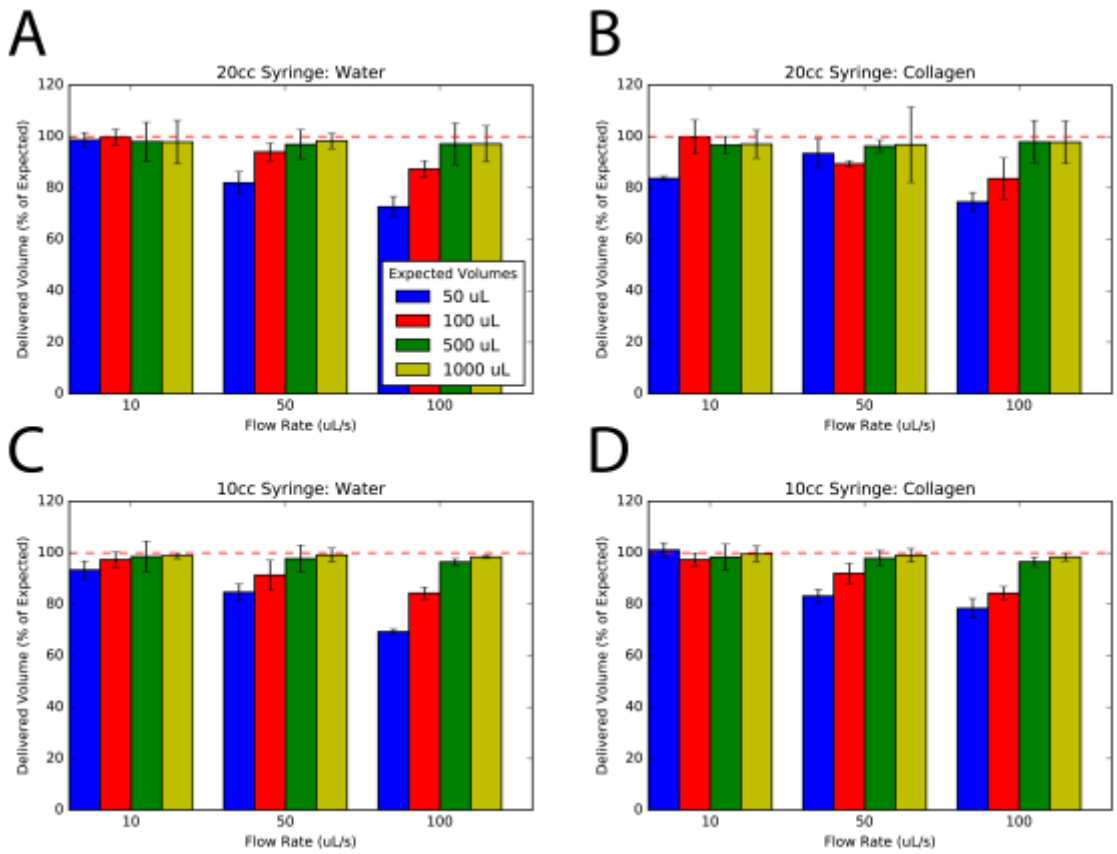

Figure 15. Single reagent dispensed volume accuracy for water (A and C), and Collagen (B and D) using 20cc (A and B) and 10cc (C and D) syringes.

While the viscosity or size of reagent reservoirs does not affect the accuracy of the dispensed reagent volume, the accuracy does decrease as the flow rate increases for the smaller volumes dispensed (50 and 100 uL). The insignificance of fluid viscosity was most likely due to the choice of syringe pumps. Lead-screw driven pumps were chosen for this initial design iteration because they are able to maintain a constant flow rate over a much larger range of viscosities than pneumatically-driven syringe pumps. Pneumatic pumps require higher applied pressures to move higher-viscosity materials, as this requires more force. Lead-screw driven pumps are able to maintain a very high constant force, which facilitates more accurate fluid displacement over a broader range of viscosities. Because there was no significant difference between syringe

sizes, this indicates that this system could benefit from larger reagent reservoirs; as this would lead to replacing empty syringe reservoirs less frequently.

The significant difference in the interaction effect points to an inherent limitation of the pumping system. Lead-screw driven syringe pumps are not designed for the precise dispensing of small volumes of fluids. These pumps are designed to maintain a constant flow rate, usually on the order of uL/min, for hours at a time. This was made apparent by the pumps range of programmable dispensing time, from hours to tenths of seconds. Operating at the very lowest of the range of dispensing times most likely lead to this dispensing volume inaccuracy.

Table 3. Significance of each variable for both water and oligomer dispensed volume accuracy experiments and the statistical difference between the fluids themselves. ($p < 0.05$ denotes statistical significance)

Fluid	Water				Oligomer				
Variable	Syringe	Volume	Flow	Vol* Flow	Syringe	Volume	Flow	Vol* Flow	Fluid
p-value	0.33	< 0.05	< 0.05	< 0.05	0.21	< 0.05	< 0.05	< 0.05	0.86

Dispensed volume accuracy revealed inaccurate S.A.R delivery during simultaneous reagent pumping

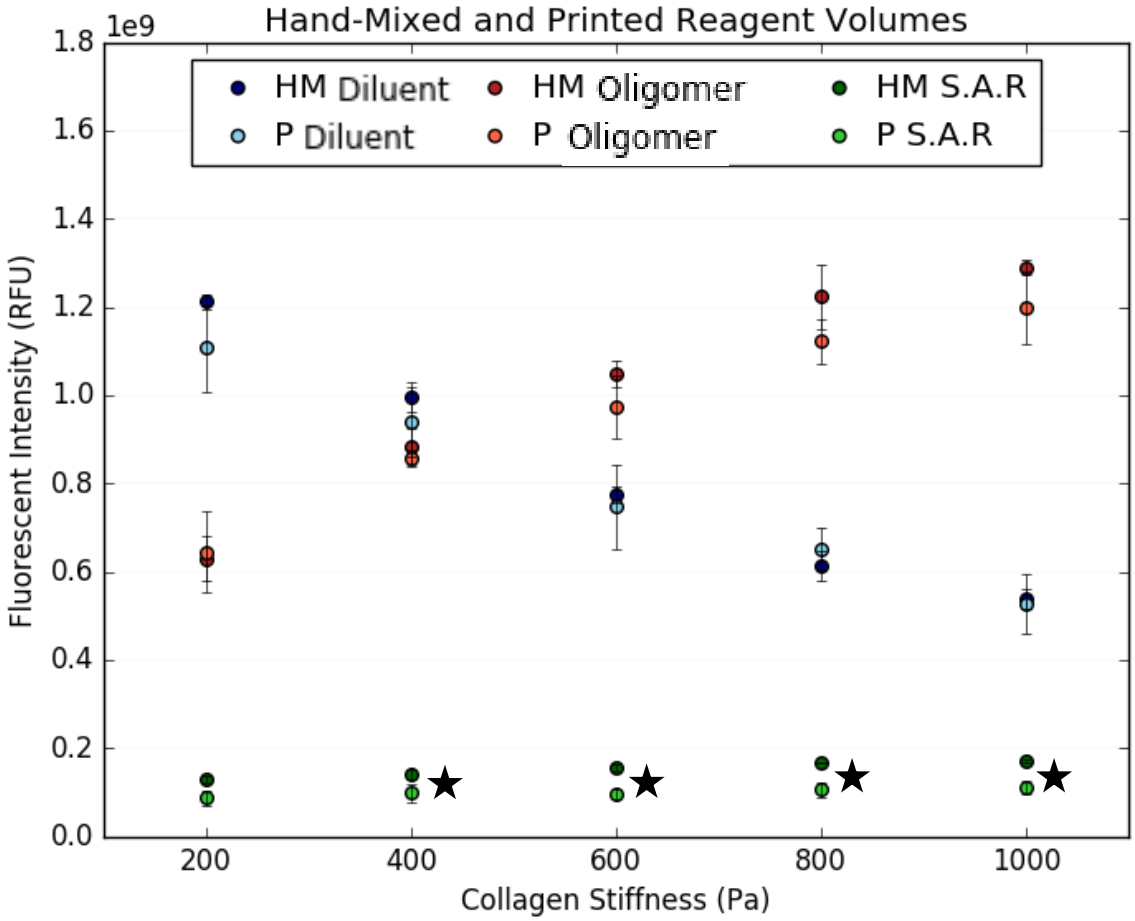

Figure 16. Fluorescent values for each reagent in hand-mixed and printed samples. ★ Denotes significance ($p < 0.05$).

Table 4. p-values comparing fluorescent intensity of printed samples to hand-mixed samples, for each reagent, and target stiffness. ($p < 0.05$ denotes statistical significance)

	200	400	600	800	1000
Diluent	0.217	0.37	0.671	0.317	0.819
Oligomer	0.814	0.487	0.236	0.145	0.198
S.A.R	0.064	0.043*	0.006*	0.027*	0.02*

Both diluent and oligomer were able to be dispensed accurately (>90%); however, the volume of S.A.R dispensed was significantly less than hand-mixed

samples (Figure 16, Table 3). This could be explained by a limitation in the pumping system. The total volume of S.A.R dispensed was much lower than that of diluent or oligomer, and the pumping system was not designed to accurately pump small volumes of fluid at high pressures for short durations (as seen in the single regent volume accuracy data), and into other streams of pressurized fluid. This could have resulted in the significant decrease in S.A.R delivery into the final samples.

Table 5. Dispensed volume accuracy, precision and mixing quality for printed samples.

	Diluent	Oligomer	S.A.R
Accuracy	94.50%	94.10%	53.20%
Precision	± 7.6%	± 5.1%	± 12.3%
Mixing Quality	0.1	0.07	0.17

The mixing quality and precision of printed samples were both lower than that of hand-mixed samples (Table 5). Mixing quality of hand-mixed samples were less than 5%, indicating a well-mixed fluid. This result partially validated the experimental method, and was used as the gold standard. Mixing quality of the printed samples was lower than that of hand-mixed samples. Furthermore, the measured decrease in precision seen in printed samples indicated a need for a more precise, reliable pumping system.

Table 6. Mixing Quality and Precision of printed samples compared to hand-mixed samples.

		Diluent	Oligomer	S.A.R
Hand-Mixed	Mixing Quality	0.033	0.046	0.043
	Precision	± 2.40%	± 3.40%	± 3.10%

Table 6 Continued.

Printed	Mixing Quality	0.1	0.07	0.17
	Precision	± 7.60%	± 5.10%	± 12.30%

Shear storage modulus of printed samples are similar to hand-mixed samples

Table 7. Shear storage modulus (G') of hand-mixed and printed samples. * Indicates significance ($\alpha < 0.05$).

Target Stiffness (Pa)	1000	800	600	400	200
Hand-Mixed	1109 ± 59*	861 ± 24	620 ± 29*	375 ± 49	199 ± 8.7*
Printed	703 ± 86*	698 ± 67	480 ± 44*	344 ± 48	171 ± 3.5*

Table 8. Statistical analysis of the difference between shear storage modulus of hand-mixed and printed samples.

Target Stiffness	1000	800	600	400	200
p-value	< 0.05	0.058	< 0.05	0.475	< 0.05

For all concentrations tested, the shear storage modulus of printed samples was lower than that of hand-mixed samples (Table 6). The most likely cause for this decrease in mechanical stiffness is the decrease in S.A.R dispensed in the printed samples (Table 5). The S.A.R is responsible for the neutralization of the final collagen sample. If the final pH of the collagen sample did not reach neutral levels (due to a decrease in S.A.R in the mixture), this would have led to the

incomplete polymerization of samples; thus, resulting in lower stiffness values. G' of printed samples does approach hand-mixed and target values in the lower stiffness range (200 – 400 Pa). This could be a result of interaction effects between S.A.R and the flow of oligomer, which increases as the target stiffness increases, possibly making it more difficult for the relatively small amount of S.A.R to be dispensed properly.

The bioprinting nozzle is able to dispense a gradient of collagen concentration within the same tissue construct

The microstructure of the 3 mL gradient tissue construct was analyzed using reflectance imaging. The resulting fibril structures indicate that one end of the tissue construct had a lower fibril density than the opposing side, and in between the two extremes, a fibril density that is an average of the two, as shown in Figure 17.

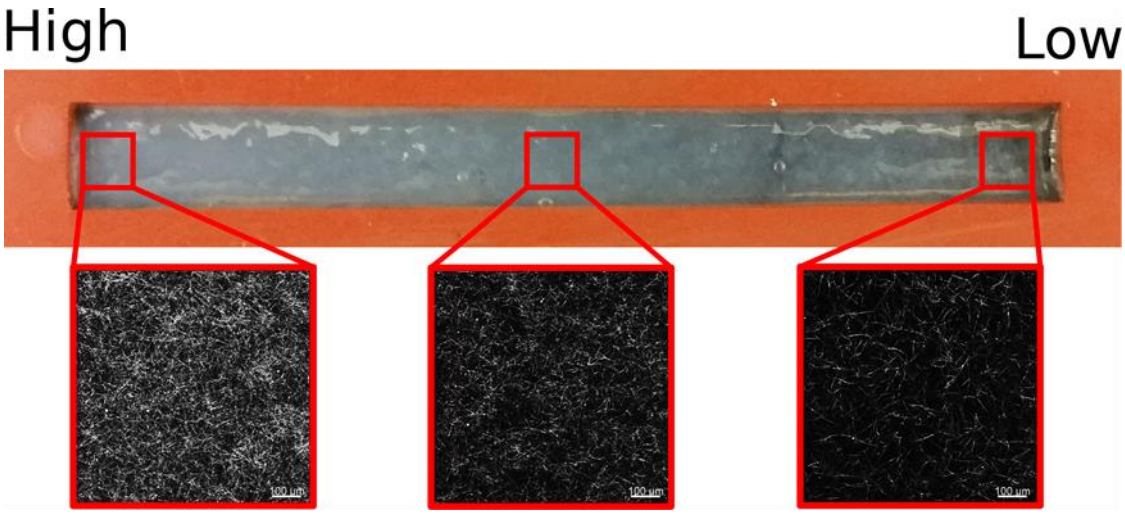

Figure 17. Tissue construct in fabricated well, with confocal reflectance images of the collagen microstructure taken at three locations along the length.

Bioprinter mixing process does not affect cell viability

Cell viability of printed cells in media was not significantly different than the negative control (Figure 10). This indicates that the narrowing of the side channel, mixing of the fluid in the mixing chamber, and final extrusion through the needle, did not cause enough shear force to significantly affect the cell viability of fibroblasts. Furthermore, there was no significant difference in cell viability between cells dispensed at any of the tested flow rates, suggesting that flow rate could be increased without having a deleterious effect on cell health. Increasing the flow rate could be considered in later iterations of this design to increase mixing quality.

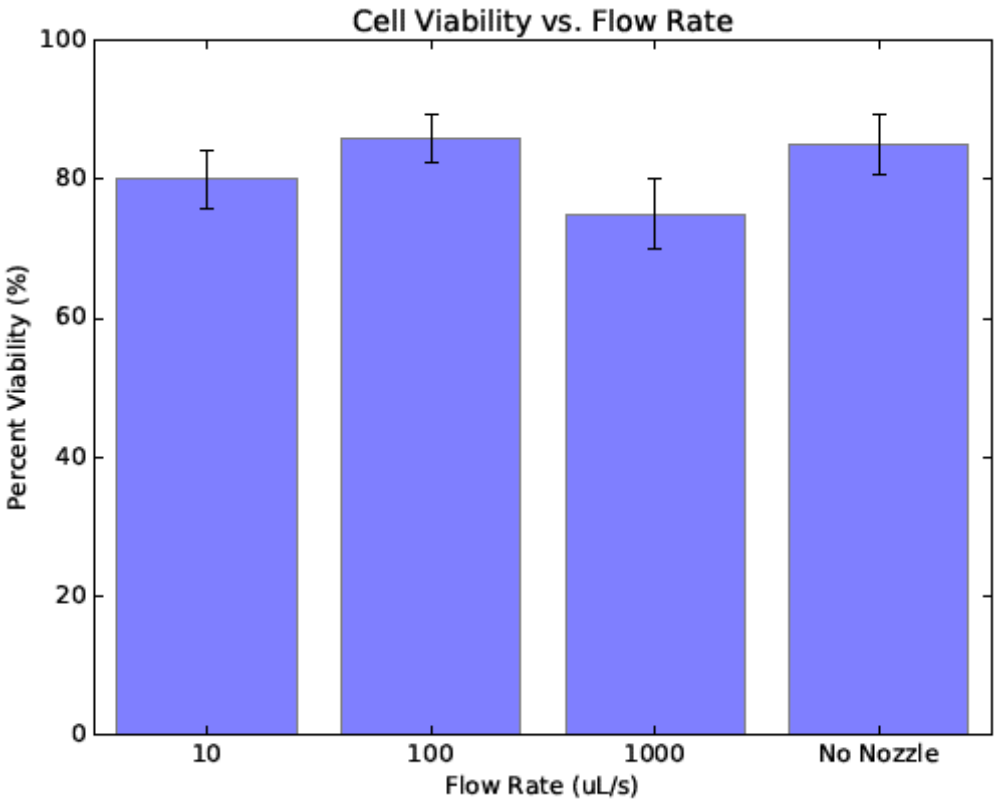

Figure 18. Viability of cells printed at 10, 100, and 1000 µL/s compared to the positive and negative controls. All experimental groups were statistically equivalent ($p < 0.05$).

For this experiment, a 3cc syringe was used after the previous attempts of using a 10cc syringe were done for 10 and 100 uL/sec resulted in low cell density measured, as shown in table 9. After changing to the 3cc syringe, cell densities improved.

Table 9. Average cell viabilities for each flow condition, the standard deviation, and the statistical significance of the average cell viability of each flow condition compared to the cells not dispensed through the mixer. ($p < 0.05$ denotes statistical significance)

	Flow Condition			
	10 µL/s	100 µL/s	1000 µL/s	Starting Cell Suspension
Cell Viability	80%	86%	75%	85%
Stdev.	4.2	3.5	5.1	4.3
p-value	0.373	0.78	0.224	-

Table 10. Cell density results for 10cc syringe and 3cc syringe sizes.

Syringe Volume	10cc			3cc			
Flow Rate (µL/s)	10	100	1000	10	100	1000	Starting Cell Suspension
Cells / mL	85,926	58,889	-	408,148	476,296	440,740	450,370

The hypothesized reason for these low cell densities was cell settling in the media. The syringe with cells in media was placed horizontally on the syringe pump, and it was thought that after the time taken to calculate the cell viability of three samples of printed solution, the remaining cells in the reservoir had sunk to

the bottom edge of the syringe. When the next samples were dispensed from the collagen, the majority of cells had settled to the bottom of the syringe, resulting in decreased cell densities.

To overcome problems with cell settling, a 3cc syringe was used so that after three samples had been printed and measured for cell viability, the stock solution was mixed, and 2 mL was taken into the syringe and immediately printed. This approach reduced the time that cells were in the reservoirs, and resulted in higher cell densities, and more repeatable results.

CHAPTER 4. CONCLUSIONS AND FUTURE WORK

Implications for fluidic mixing 3D bioprinters

The experiments presented in this study have proven the potential for a fluidic mixing nozzle that can dispense a broad range of ECM concentrations in a single tissue construct. The mixing nozzle prototype was able to dispense accurate volumes of two of the three reagents needed for oligomeric type I collagen during simultaneous pumping, but dispensed significantly less S.A.R than was required. The nozzle was found to create collagen samples that were similar to the stiffness of hand-mixed samples, was able to print a gradient of collagen concentrations in the same tissue construct, and was found to not significantly decrease cell viability of printed fibroblasts.

Limitations needed to be addressed for the next prototype iteration

Limitations of the pumping system contributed to inaccurate volumes of dispensed reagents, as seen directly from the dispensed volume accuracy data. This effect was negated as much as possible by choosing a flow rate that had been measured to be the most accurate during single reagent dispensing, but a new pumping system that is designed for small volume fluid dispensing will need to be procured for the next iteration of the mixing nozzle prototype.

Fluorescence data measured that the mixing quality of printed volume fraction samples was less than those of hand-mixed samples, as well as precision of reagent volume dispensed. This again raises the need for a pumping system designed for this specific application. Mixing quality and precision should increase with a pumping system that can dispense the correct volume of

reagents during simultaneous dispensing. Increasing the flow rate of the reagents would also improve mixing quality, but would need to be balanced by the effect it would have on cell viability.

Final stiffness values of samples printed were lower than those of hand-mixed samples, and in conjunction with the reagent volume data, was explained by the lack of S.A.R in printed samples. A more accurate pumping system and would account for the differences seen between printed and hand-mixed volume fraction samples for the rheometric experiment. Accurate pumping will ensure that the correct amount of reagents are being dispensed, leading to the complete neutralization.

The cell viability results suggested that this method of mixing and combining fluids does not decrease cell viability significantly from cells not extruded through the nozzle. Further experiments using cells encapsulated in oligomeric collagen may provide a more relevant result regarding the cell viability of cells printed in collagen, as this is the environment the cells would be encapsulated in the mixing chamber and being extruded through the nozzle.

Future Work

The results presented in this thesis identify future design improvements and experiment design that need to be completed to further the next prototype design. Specific areas of investigation include 1) Improving the reagent pumping system, 2) Reliable temperature control, 3) Direct quantification of fluidic mixing quality and efficiency, and 4) More relevant cell viability studies. By addressing these questions with specifically designed experiments, we can provide thorough validation results for the next bioprinting nozzle, and build off of the key findings from this research.

Firstly, a new pumping system should replace the current setup, as the current setup was meant to serve as a proof-of-concept, and was never intended

to be a final solution. The new pumping system should be designed to deliver very small volumes of reagents against a high-pressure. Metering pumps or similar systems might prove to be the best option for the next design of nozzle. This will allow for the correct volumes of each reagent to be dispensed, regardless of viscosity or flow rate of the other reagents being pumped into the nozzle simultaneously, which is essential for this project.

Next, full control over the reagent temperatures is needed to ensure that polymerization of the collagen does not occur in the nozzle. For this proof-of-concept design, temperature control was accomplished with direct contact with packs of ice, but this technique was difficult to manage, and constantly needed maintenance. Full temperature control could be done by machining channels into the nozzle that are pumped with chilled water- cooling the nozzle. Cooling of the syringe reservoirs should also help ameliorate any foreseeable issue.

The direct quantification of fluidic mixing quality and efficiency is paramount in the next version of the bioprinting nozzle. To do this, a new testing method must be developed to directly, and more accurately, measure the mixing quality and efficiency of each reagent. Using this test, optimization of flow rates and mixing strategies could be undergone to achieve a desired mixing quality, and improve mixing efficiency.

More relevant cell studies are needed to accurately predict the cell viability of printed cells in oligomeric collagen. The current cell viability studies were done with cell media, which has a much lower viscosity than the oligomeric collagen. This difference in viscosity may result in differences in cell viability. Different cell types should also be printed, as certain cell types are more sensitive to shear forces.

LIST OF REFERENCES

REFERENCES

Abraham, L. C., Zuena, E., Perez-Ramirez, B., & Kaplan, D. L. (2008). Guide to collagen characterization for biomaterial studies. Journal of Biomedical Materials Research Part B: Applied Biomaterials, 87(1), 264-285.

ASTM F3089-14, Standard Guide for Characterization and Standardization of Polymerizable Collagen-Based Products and Associated Collagen-Cell Interactions, ASTM International, West Conshohocken, PA, 2014, www.astm.com

Bailey, J. L., Critser, P. J., Whittington, C., Kuske, J. L., Yoder, M. C., & Voytik-Harbin, S. L. (2011). Collagen oligomers modulate physical and biological properties of three-dimensional self-assembled matrices. Biopolymers, 95(2), 77-93.

Balgude, A. P., Yu, X., Szymanski, A., & Bellamkonda, R. V. (2001). Agarose gel stiffness determines rate of DRG neurite extension in 3D cultures. Biomaterials, 22(10), 1077-1084.

Bertassoni, L. E., Cardoso, J. C., Manoharan, V., Cristino, A. L., Bhise, N. S., Araujo, W. A., ... & Khademhosseini, A. (2014). Direct-write bioprinting of cell-laden methacrylated gelatin hydrogels. Biofabrication, 6(2), 024105.

Bertassoni, L. E., Cecconi, M., Manoharan, V., Nikkhah, M., Hjortnaes, J., Cristino, A. L., ... & Khademhosseini, A. (2014). Hydrogel bioprinted microchannel networks for vascularization of tissue engineering constructs. Lab on a Chip, 14(13), 2202-2211.

Blum, K. M., Novak, T., Watkins, L., Neu, C. P., Wallace, J. M., Bart, Z. R., & Voytik-Harbin, S. L. (2016). Acellular and cellular high-density, collagen-fibril constructs with suprafibrillar organization. Biomaterials science

Brightman, A. O., Rajwa, B. P., Sturgis, J. E., McCallister, M. E., Robinson, J. P., & Voytik-Harbin, S. L. (2000). Time-lapse confocal reflection microscopy of collagen fibrillogenesis and extracellular matrix assembly in vitro. Biopolymers, 54(3), 222-234.Chandrakasan, G., Torchia, D. A., & Piez, K. A. (1976). Preparation of intact monomeric collagen from rat tail tendon and skin and the structure of the nonhelical ends in solution. Journal of Biological Chemistry, 251(19), 6062-6067.

Chang, C. C., Boland, E. D., Williams, S. K., & Hoying, J. B. (2011). Direct-write bioprinting three-dimensional biohybrid systems for future regenerative therapies. Journal of Biomedical Materials Research Part B: Applied Biomaterials, 98(1), 160-170.Chang, R., Nam, J., & Sun, W. (2008). Effects of dispensing pressure and nozzle diameter on cell survival from solid freeform fabrication-based direct cell writing. Tissue Engineering Part A, 14(1), 41-48.

Cui, X., Boland, T., D'Lima, D. D., & Lotz, M. K. (2012). Thermal inkjet printing in tissue engineering and regenerative medicine. Recent patents on drug delivery & formulation, 6(2), 149.

Cui, X., Breitenkamp, K., Finn, M. G., Lotz, M., & D'Lima, D. D. (2012). Direct human cartilage repair using three-dimensional bioprinting technology. Tissue Engineering Part A, 18(11-12), 1304-1312.

Dreher, S., Kockmann, N., & Woias, P. (2009). Characterization of laminar transient flow regimes and mixing in T-shaped micromixers. *heat transfer engineering*, *30*(1-2), 91-100.

Duan, B., Hockaday, L. A., Kang, K. H., & Butcher, J. T. (2013). 3D bioprinting of heterogeneous aortic valve conduits with alginate/gelatin hydrogels. Journal of Biomedical Materials Research Part A, 101(5), 1255-1264.

Duocastella, M., Colina, M., Fernández-Pradas, J. M., Serra, P., & Morenza, J. L. (2007). Study of the laser-induced forward transfer of liquids for laser bioprinting. Applied surface science, 253(19), 7855-7859.

Fedorovich, N. E., De Wijn, J. R., Verbout, A. J., Alblas, J., & Dhert, W. J. (2008). Three-dimensional fiber deposition of cell-laden, viable, patterned constructs for bone tissue printing. Tissue Engineering Part A, 14(1), 127-133.

Fedorovich, N. E., Swennen, I., Girones, J., Moroni, L., Van Blitterswijk, C. A., Schacht, E., ... & Dhert, W. J. (2009). Evaluation of photocrosslinked lutrol hydrogel for tissue printing applications. Biomacromolecules, 10(7), 1689-1696.

Friedl, P., Zänker, K. S., & Bröcker, E. B. (1998). Cell migration strategies in 3-D extracellular matrix: differences in morphology, cell matrix interactions, and integrin function. Microscopy research and technique, 43(5), 369-378.

Gaebel, R., Ma, N., Liu, J., Guan, J., Koch, L., Klopsch, C., ... & Wang, F. (2011). Patterning human stem cells and endothelial cells with laser printing for cardiac regeneration. Biomaterials, 32(35), 9218-9230.

Gao, Q., He, Y., Fu, J. Z., Liu, A., & Ma, L. (2015). Coaxial nozzle-assisted 3D bioprinting with built-in microchannels for nutrients delivery. Biomaterials,61, 203-215.

Gauvin, R., Chen, Y. C., Lee, J. W., Soman, P., Zorlutuna, P., Nichol, J. W., ... & Khademhosseini, A. (2012). Microfabrication of complex porous tissue engineering scaffolds using 3D projection stereolithography. Biomaterials, 33(15), 3824-3834.

Georges, P. C., & Janmey, P. A. (2005). Cell type-specific response to growth on soft materials. Journal of applied physiology, 98(4), 1547-1553.

Gobby, D., Angeli, P., & Gavriilidis, A. (2001). Mixing characteristics of T-type microfluidic mixers. Journal of Micromechanics and microengineering, 11(2), 126.

Gómez-Guillén, M. C., Giménez, B., López-Caballero, M. A., & Montero, M. P. (2011). Functional and bioactive properties of collagen and gelatin from alternative sources: A review. Food Hydrocolloids, 25(8), 1813-1827.

Gu, L., & Mooney, D. J. (2016). Biomaterials and emerging anticancer therapeutics: engineering the microenvironment. Nature Reviews Cancer, 16(1), 56-66.

Guillemot, F., Souquet, A., Catros, S., Guillotin, B., Lopez, J., Faucon, M., ... & Chabassier, P. (2010). High-throughput laser printing of cells and biomaterials for tissue engineering. Acta biomaterialia, 6(7), 2494-2500.

Guillotin, B., Souquet, A., Catros, S., Duocastella, M., Pippenger, B., Bellance, S., ... & Guillemot, F. (2010). Laser assisted bioprinting of engineered tissue with high cell density and microscale organization. Biomaterials, 31(28), 7250-7256.

Günther, A., & Jensen, K. F. (2006). Multiphase microfluidics: from flow characteristics to chemical and materials synthesis. *Lab on a Chip*, *6*(12), 1487-1503.

Hadjipanayi, E., Mudera, V., & Brown, R. A. (2009). Guiding cell migration in 3D: a collagen matrix with graded directional stiffness. Cell motility and the cytoskeleton, 66(3), 121-128.

Horváth, L., Umehara, Y., Jud, C., Blank, F., Petri-Fink, A., & Rothen-Rutishauser, B. (2015). Engineering an in vitro air-blood barrier by 3D bioprinting. Scientific reports, 5.

Hourd, P., Medcalf, N., Segal, J., & Williams, D. J. (2015). A 3D bioprinting exemplar of the consequences of the regulatory requirements on customized processes. Regenerative medicine, 10(7), 863-883.

Jakab, K., Neagu, A., Mironov, V., Markwald, R. R., & Forgacs, G. (2004). Engineering biological structures of prescribed shape using self-assembling multicellular systems. Proceedings of the National Academy of Sciences of the United States of America, 101(9), 2864-2869.

Jakab, K., Norotte, C., Damon, B., Marga, F., Neagu, A., Besch-Williford, C. L., ... & Markwald, R. (2008). Tissue engineering by self-assembly of cells printed into topologically defined structures. Tissue Engineering Part A,14(3), 413-421.

Jakab, K., Norotte, C., Marga, F., Murphy, K., Vunjak-Novakovic, G., & Forgacs, G. (2010). Tissue engineering by self-assembly and bio-printing of living cells. Biofabrication, 2(2), 022001.

Jang, J., Kim, T. G., Kim, B. S., Kim, S. W., Kwon, S. M., & Cho, D. W. (2016). Tailoring Mechanical Properties of Decellularized Extracellular Matrix Bioink by Vitamin B2-induced Photo-crosslinking. Acta Biomaterialia.

Justin, R. T., & Engler, A. J. (2011). Stiffness gradients mimicking in vivo tissue variation regulate mesenchymal stem cell fate. PloS one, 6(1), e15978.

Kang, H. W., Lee, S. J., Ko, I. K., Kengla, C., Yoo, J. J., & Atala, A. (2016). A 3D bioprinting system to produce human-scale tissue constructs with structural integrity. Nature biotechnology, 34(3), 312-319.

Khalil, S., & Sun, W. (2007). Biopolymer deposition for freeform fabrication of hydrogel tissue constructs. Materials Science and Engineering: C, 27(3), 469-478.

Kolesky, D. B., Truby, R. L., Gladman, A., Busbee, T. A., Homan, K. A., & Lewis, J. A. (2014). 3D bioprinting of vascularized, heterogeneous cell-laden tissue constructs. Advanced materials, 26(19), 3124-3130.

Kreger, S. T., Bell, B. J., Bailey, J., Stites, E., Kuske, J., Waisner, B., & Voytik-Harbin, S. L. (2010). Polymerization and matrix physical properties as important design considerations for soluble collagen formulations. Biopolymers, 93(8), 690-707.

Lee, C. H., Singla, A., & Lee, Y. (2001). Biomedical applications of collagen. International journal of pharmaceutics, 221(1), 1-22.

Lee, H., Yoo, J. J., Kang, H. W., & Cho, D. W. (2016). Investigation of thermal degradation with extrusion-based dispensing modules for 3D bioprinting technology. Biofabrication, 8(1), 015011.

Lee, J. S., Hong, J. M., Jung, J. W., Shim, J. H., Oh, J. H., & Cho, D. W. (2014). 3D printing of composite tissue with complex shape applied to ear regeneration. Biofabrication, 6(2), 024103.

Lee, K. Y., & Mooney, D. J. (2012). Alginate: properties and biomedical applications. Progress in polymer science, 37(1), 106-126.

Lodish H, Berk A, Zipursky SL, et al. (2000). Section 22.3 Collagen: The Fibrous Proteins of the Matrix. W. H. Freeman (4), Molecular Cell Biology. http://www.ncbi.nlm.nih.gov/books/NBK21582/

Lu, P., Weaver, V. M., & Werb, Z. (2012). The extracellular matrix: a dynamic niche in cancer progression. The Journal of cell biology, 196(4), 395-406.

Markstedt, K., Mantas, A., Tournier, I., Martínez Ávila, H., Hägg, D., & Gatenholm, P. (2015). 3D Bioprinting Human Chondrocytes with Nanocellulose–Alginate Bioink for Cartilage Tissue Engineering Applications. Biomacromolecules, 16(5), 1489-1496.

Mason, B. N., Starchenko, A., Williams, R. M., Bonassar, L. J., & Reinhart-King, C. A. (2013). Tuning three-dimensional collagen matrix stiffness independently of collagen concentration modulates endothelial cell behavior. Acta biomaterialia, 9(1), 4635-4644.

Mézel, C., Souquet, A., Hallo, L., & Guillemot, F. (2010). Bioprinting by laser-induced forward transfer for tissue engineering applications: jet formation modeling. Biofabrication, 2(1), 014103.

Mironov, V., Reis, N., & Derby, B. (2006). Review: bioprinting: a beginning. Tissue engineering, 12(4), 631-634.

Murphy, S. V., & Atala, A. (2014). 3D bioprinting of tissues and organs.*Nature biotechnology*, *32*(8), 773-785.

Murphy, S. V., Skardal, A., & Atala, A. (2013). Evaluation of hydrogels for bio-printing applications. Journal of Biomedical Materials Research Part A, 101(1), 272-284.

Ng, W. L., Yeong, W. Y., & Naing, M. W. (2016). Polyelectrolyte gelatin-chitosan hydrogel optimized for 3D bioprinting in skin tissue engineering. International Journal of Bioprinting, 2.

Norotte, C., Marga, F. S., Niklason, L. E., & Forgacs, G. (2009). Scaffold-free vascular tissue engineering using bioprinting. Biomaterials, 30(30), 5910-5917.

Ozbolat, I. T., & Hospodiuk, M. (2016). Current advances and future perspectives in extrusion-based bioprinting. Biomaterials, 76, 321-343.

Ozbolat, I. T., & Yu, Y. (2013). Bioprinting toward organ fabrication: challenges and future trends. Biomedical Engineering, IEEE Transactions on, 60(3), 691-699.

Ozbolat, I. T., Chen, H., & Yu, Y. (2014). Development of 'Multi-arm Bioprinter'for hybrid biofabrication of tissue engineering constructs. Robotics and Computer-Integrated Manufacturing, 30(3), 295-304.

Pati, F., Jang, J., Ha, D. H., Kim, S. W., Rhie, J. W., Shim, J. H., ... & Cho, D. W. (2014). Printing three-dimensional tissue analogues with decellularized extracellular matrix bioink. Nature communications, 5.

Rimann, M., & Graf-Hausner, U. (2012). Synthetic 3D multicellular systems for drug development. Current opinion in biotechnology, 23(5), 803-809.

Rodrigues, A. I., Gomes, M. E., Leonor, I. B., & Reis, R. L. (2012). Bioactive starch-based scaffolds and human adipose stem cells are a good combination for bone tissue engineering. Acta biomaterialia, 8(10), 3765-3776.

Rowley, J. A., Madlambayan, G., & Mooney, D. J. (1999). Alginate hydrogels as synthetic extracellular matrix materials. Biomaterials, 20(1), 45-53.

Rutz, A. L., Hyland, K. E., Jakus, A. E., Burghardt, W. R., & Shah, R. N. (2015). A Multimaterial Bioink Method for 3D Printing Tunable, Cell-Compatible Hydrogels. Advanced Materials, 27(9), 1607-1614.

Sachan, N. K., Pushkar, S., Jha, A., & Bhattcharya, A. (2009). Sodium alginate: the wonder polymer for controlled drug delivery. J Pharm Res, 2(8), 1191-9.

Sano, A., Maeda, M., Nagahara, S., Ochiya, T., Honma, K., Itoh, H., ... & Fujioka, K. (2003). Atelocollagen for protein and gene delivery. Advanced drug delivery reviews, 55(12), 1651-1677.

Saunders, R. E., Gough, J. E., & Derby, B. (2008). Delivery of human fibroblast cells by piezoelectric drop-on-demand inkjet printing. Biomaterials, 29(2), 193-203.

Schuurman, W., Khristov, V., Pot, M. W., Van Weeren, P. R., Dhert, W. J. A., & Malda, J. (2011). Bioprinting of hybrid tissue constructs with tailorable mechanical properties. Biofabrication, 3(2), 021001.

Seidi, A., Ramalingam, M., Elloumi-Hannachi, I., Ostrovidov, S., & Khademhosseini, A. (2011). Gradient biomaterials for soft-to-hard interface tissue engineering. Acta biomaterialia, 7(4), 1441-1451.

Shamloo, A., & Heilshorn, S. C. (2010). Matrix density mediates polarization and lumen formation of endothelial sprouts in VEGF gradients. Lab on a Chip, 10(22), 3061-3068.

Shim, J. H., Kim, J. Y., Park, M., Park, J., & Cho, D. W. (2011). Development of a hybrid scaffold with synthetic biomaterials and hydrogel using solid freeform fabrication technology. Biofabrication, 3(3), 034102.

Shim, J. H., Lee, J. S., Kim, J. Y., & Cho, D. W. (2012). Bioprinting of a mechanically enhanced three-dimensional dual cell-laden construct for osteochondral tissue engineering using a multi-head tissue/organ building system. Journal of Micromechanics and Microengineering, 22(8), 085014.

Skardal, A., Mack, D., Kapetanovic, E., Atala, A., Jackson, J. D., Yoo, J., & Soker, S. (2012). Bioprinted amniotic fluid-derived stem cells accelerate healing of large skin wounds. Stem cells translational medicine, 1(11), 792.

Skardal, A., Zhang, J., & Prestwich, G. D. (2010). Bioprinting vessel-like constructs using hyaluronan hydrogels crosslinked with tetrahedral polyethylene glycol tetracrylates. Biomaterials, 31(24), 6173-6181.

Skardal, A., Zhang, J., McCoard, L., Xu, X., Oottamasathien, S., & Prestwich, G. D. (2010). Photocrosslinkable hyaluronan-gelatin hydrogels for two-step bioprinting. Tissue Engineering Part A, 16(8), 2675-2685.

Smith, C. M., Christian, J. J., Warren, W. L., & Williams, S. K. (2007). Characterizing environmental factors that impact the viability of tissue-engineered constructs fabricated by a direct-write bioassembly tool. Tissue engineering, 13(2), 373-383.

Smith, C. M., Stone, A. L., Parkhill, R. L., Stewart, R. L., Simpkins, M. W., Kachurin, A. M., ... & Williams, S. K. (2004). Three-dimensional bioassembly tool for generating viable tissue-engineered constructs. Tissue engineering,10(9-10), 1566-1576.

Statiflo Static Mixers, Channel Mixers and Motionless Mixing Technology. (n.d.). Retrieved March 22, 2016, from http://www.statiflo.com/en/about-static-mixing/mixture-quality/146-the-difference-between-mixer-efficiency-and-mixture-quality

Stenzel, K. H., Miyata, T., & Rubin, A. L. (1974). Collagen as a biomaterial. Annual review of biophysics and bioengineering, 3(1), 231-253.

Strober, W. (2001). Trypan blue exclusion test of cell viability. Current protocols in immunology, A3-B.

Suri, S., Han, L. H., Zhang, W., Singh, A., Chen, S., & Schmidt, C. E. (2011). Solid freeform fabrication of designer scaffolds of hyaluronic acid for nerve tissue engineering. Biomedical microdevices, 13(6), 983-993.

Tan, E. Y. S., & Yeong, W. Y. (2015). Concentric bioprinting of alginate-based tubular constructs using multi-nozzle extrusion-based technique. International Journal of Bioprinting, 1.

Tan, Y. S. E., & Yeong, W. Y. (2014). Direct bioprinting of alginate-based tubular constructs using multi-nozzle extrusion-based technique. In 1st International Conference on Progress in Additive Manufacturing.

Thakur, R. K., Vial, C., Nigam, K. D. P., Nauman, E. B., & Djelveh, G. (2003). Static mixers in the process industries—a review. *Chemical Engineering Research and Design*, *81*(7), 787-826.

Vanarase, A. U., Alcalà, M., Rozo, J. I. J., Muzzio, F. J., & Romañach, R. J. (2010). Real-time monitoring of drug concentration in a continuous powder mixing process using NIR spectroscopy. *Chemical Engineering Science*,*65*(21), 5728-5733.

Van Den Bulcke, A. I., Bogdanov, B., De Rooze, N., Schacht, E. H., Cornelissen, M., & Berghmans, H. (2000). Structural and rheological properties of methacrylamide modified gelatin hydrogels. Biomacromolecules, 1(1), 31-38.

Wang, N., Butler, J. P., & Ingber, D. E. (1993). Mechanotransduction across the cell surface and through the cytoskeleton. Science, 260(5111), 1124-1127.

Wells, R. G. (2008). The role of matrix stiffness in regulating cell behavior. Hepatology, 47(4), 1394-1400.

Whittington, C. F., Yoder, M. C., & Voytik-Harbin, S. L. (2013). Collagen-Polymer Guidance of Vessel Network Formation and Stabilization by Endothelial Colony Forming Cells In Vitro. Macromolecular bioscience, 13(9), 1135-1149.

Wüst, S., Godla, M. E., Müller, R., & Hofmann, S. (2014). Tunable hydrogel composite with two-step processing in combination with innovative hardware upgrade for cell-based three-dimensional bioprinting. Acta biomaterialia, 10(2), 630-640.

Yeung, T., Georges, P. C., Flanagan, L. A., Marg, B., Ortiz, M., Funaki, M., ... & Janmey, P. A. (2005). Effects of substrate stiffness on cell morphology, cytoskeletal structure, and adhesion. Cell motility and the cytoskeleton, 60(1), 24-34.

Yu, Y., Zhang, Y., & Ozbolat, I. T. (2014). A Hybrid Bioprinting Approach for Scale-Up Tissue Fabrication. Journal of Manufacturing Science and Engineering, 136(6), 061013.

Yu, Y., Zhang, Y., Martin, J. A., & Ozbolat, I. T. (2013). Evaluation of cell viability and functionality in vessel-like bioprintable cell-laden tubular channels. Journal of biomechanical engineering, 135(9), 091011.

Yue, K., Trujillo-de Santiago, G., Alvarez, M. M., Tamayol, A., Annabi, N., & Khademhosseini, A. (2015). Synthesis, properties, and biomedical applications of gelatin methacryloyl (GelMA) hydrogels. Biomaterials, 73, 254-271.

Zhang, Y., Yu, Y., Akkouch, A., Dababneh, A., Dolati, F., & Ozbolat, I. T. (2015). In vitro study of directly bioprinted perfusable vasculature conduits. Biomaterials science, 3(1), 134-143.

Zhang, Y., Yu, Y., Chen, H., & Ozbolat, I. T. (2013). Characterization of printable cellular micro-fluidic channels for tissue engineering. Biofabrication,5(2), 025004.